2016

Drying Methods for the Fabrication of Polymer Foam Material

Dalton Echard

www.manaraa.com

2016

Drying Methods for the Fabrication of Polymer Foam Material

Dalton Echard
Virginia Commonwealth University

Follow this and additional works at: http://scholarscompass.vcu.edu/etd

Part of the Physics
Commons

© The Author

Downloaded from

Drying Methods for the Fabrication of Polymer Aerogel Material

A thesis submitted in partial fulfillment of the requirements for the degree of Master of Science in Physics / Applied Physics at Virginia Commonwealth University.

By

Dalton R. Echard

B.S. in Physics

University of Mary Washington, 2014

M.S. in Physics/Applied Physics

Virginia Commonwealth University, 2016

Director Massimo F. Bertino

Professor, Department of Physics

Virginia Commonwealth University,

Richmond, Virginia, 2328

4-18-2016

Acknowledgements

Massimo Bertino, for being a "loving" and "caring" director who really allowed me to learn hands on and pushed me to go out of my comfort zone

The Nano and Physics departments, for all aid and classroom education

Gerd Langenbucher of Anton Paar, for allowing us to take SAXS measurements and aiding on the device.

A Special thanks to Berteamo, for all your support and help through the years. You made it almost enjoyable to be here.

Table of Contents

Drying Methods for the Fabrication of Polymer Foam Material

By Dalton Echard

A thesis submitted in partial fulfillment of the requirements of the degree of Master of Science at Virginia Commonwealth University.

Virginia Commonwealth University, 2016

Major Director: Dr. Massimo Bertino

Professor, VCU Department of Physics

ABSTRACT

This is a report on the study of the drying of nanoporous polymer foam material fabricated by photolithogtaphic methods. Three drying methods were employed, which were air drying, supercritical drying and freeze drying. After fabrication and drying, physical properties of the polymer foams were measured. These measurements included density of the material, Young's modulus, surface area, and the shape of the skeletal particles. The measurements determined the effect of the polymer concentration and the effect of drying methods. It was determined that polymer concentration had a much larger effect on the properties of the materials than the drying method.

Chapter 1: Introduction and History

1.1) History of aerogel/foams

In 1932 the term aerogel was first used by Kistler. [1-3] Aerogel is a material where a gel containing liquid has the liquid replaced with gas while still maintaining the structure and volume of the original gel. Initially, the solvent in aerogels were difficult to remove, and drying was done by evaporation. This was soon after improved upon by using the supercritical drying technique. [1] Aerogels are a type of nanoporous foam which consists of nanoparticles aggregated into larger secondary particles. The structure is highly porous, and has two types of pores; micropores, which are the pores between primary particles, and mesopores which are the pores between secondary particles. Figure 1 Shows a schematic representation of an aerogel, along with a macroscopic analogy; a cauliflower.
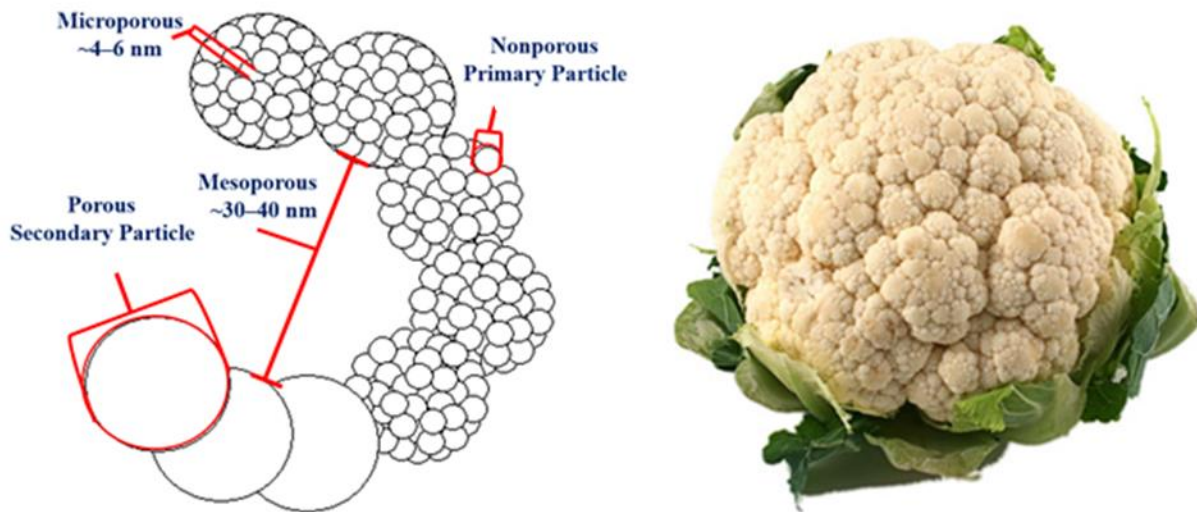

Figure 1. Right: A schematic representation of the structure of an aerogel describing micro and mesopores. Left: A macroscopic analogy of an aerogel. Taken from L. White [4]

Foam and aerogel material are lightweight thermal insulators which can be designed from a large array of materials. These materials, including polymers such as polyurea, can be used in the fabrication of foams. Gels made from the polymer polyurea were first described by De Vos-Biesmans in 1994. [5] Nanofoams made with polyurea, styrene or other polymers including semi-crystalline polymers, have been produced using multiple methods. These methods include bubbling CO_2, phase separation and photogelation. [6-9] No one method works for every application though. These polymer foams, regardless of the method of production, have gotten more attention in recent years for several reasons. This is because polymer nanofoams have an interesting array of properties ranging from their physical to thermal properties. [2,3,10-15] Many of these polymers such as PET have a low cost yet still a relatively high Young's Modulus. [16] A compression test to determine Young's modulus is common to determine the mechanical properties of the material such as strength. [13] A higher strength is important as fragile foams will have fewer applications. Nano porous foams are also known to be good thermal insulators. [2,3,6,10-15] Good thermal insulators will have a low thermal conductivity, λ.[6] The low thermal conductivity of a foam is due to the Knudsen effect, where if the size of a pore 'd' is smaller than the mean free path 'l' of a particle then convection is limited. [6,11] This can be seen in figure 2.
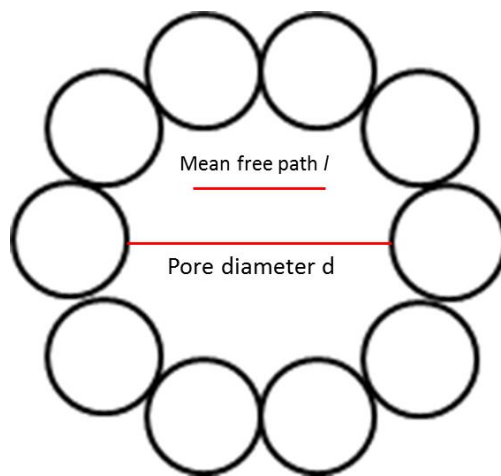

Figure 2. diagram describing the relation between the mean free path and pore size for the Knudsen effect. In this diagram convection is not limited.

This means that the nanofoams will have a lower thermal conductivity than the gas inside the pores would have alone. The thermal conductivity is function of the density. The lower the density, the lower the thermal conductivity will be as there is more pore space. [17,18] Specifically, the effective thermal conductivity, λ_{eff}, of gel or foam material is the sum of three parts. The first part is the thermal conductivity of the skeletal structure, λ_s, at room temperature and above this heat transfer is diffusive transport as a result of phonons. Because the velocity of the phonon is a function of temperature, the thermal conductivity of the solid skeletal structure is also a function of temperature. The thermal conductivity of the gas medium, λ_g, is the second component, which is a function of the pore size (Knudsen effect) which can be seen in figure 2. Finally the radiative thermal conductivity, λ_r, is also a function of temperature for a non-transparent material. [18] The equation for effective thermal conductivity is seen below.

$$\lambda_{eff} = \lambda_s + \lambda_g + \lambda_r$$

The solid skeletal structure has the largest contribution to the thermal conductivity at low temperatures (500K) while the radiate thermal conductivity has the lowest contribution in a study done by M. Wiener et al. (18) The radiative thermal conductivity remains to be a small contributor to the effective thermal conductivity up to 1770K. [18]

Some polymer foams have reported a thermal conductivity in the range of ≈0.04 W m^{-1} K^{-1} or ≈0.03 W m^{-1} K^{-1} for polystyrene and ridged polyurethane respectively. [6] Polyurea foams have had a thermal conductivity reported as low as 0.018 W m^{-1} K^{-1}. [5,17] While this is impressive, a silica aerogel will have a lower thermal conductivity still. These materials have a thermal conductivity in the range of 0.012 W m^{-1} K^{-1}. [5]

Table 1. Common nanofoam materials and their thermal conductivity

Material	Thermal conductivity in W/m·K
Polystyrene	0.04
Ridged Polyurethane	0.03
Polyurea	0.018
Silica	0.012

With all of these notable properties polymer nanofoams have a wide array of industrial uses. [13] Their low cost, paired with the high modulus some foam material possesses and their thermal properties indicate that nanoporous foams can be fantastic for thermal insulation applications including packaging. [16] Due to the size of the pores on the foams they have also been used as a catalyst support. Foams have also been used in biomedicine to deliver drugs, proteins and genes. Other applications are in electronics, microwave systems, and as absorbent material for environmental remediation. [9] The high strength of some polymers has resulted in their use in aerospace applications as a replacement for metal components. [19] Acoustic properties have also been tested indicating a high acoustic attenuation, [5] meaning they could be used to buffer sounds.

Unfortunately, aerogels and some foam materials remain difficult to produce. Their production method typically results in trouble with the drying process, [8,15] and commonly only the production of geometric shapes have been reported. [20] Additive manufacturing also has not been reported to produce custom shapes of aerogel and foam material.

Other recent research has been done by L. S. White et al. [8] who have used polymers to cross-link silica aerogels and produce a mechanically stronger material. These materials have been referred to as X-aerogels. [5] Young's Modulus has been tested for silica aerogels that were cross linked with polymers such as Hexanedioldiacrylate (HDDA) and Dipentaerythritol Hexaacrylate (DPHA). The range of modulus for these cross-linked materials was between 10-400 MPa. This is much stronger than silica aerogel material without the polymer crosslinking, which is on the order of 1 MPa. The production of these

cross-linked silica gels used a simple one pot method as well as avoiding the need for solvent exchange. These materials were then photo polymerized. [8] Since it is known this method is possible for more complex materials, it should be also possible to produce nanoporous foam using only the polymer and solvent and photo-initiators.

1.2) Sol-gel process

The sol-gel method is a synthesis procedure which is used to produce aerogel and nanofoam material. It is the process that gives these materials their appealing properties such as the high porosity and low density. [1-3] In the sol-gel method, small particles begin to aggregate to produce microscopic clusters. This is done via the process of hydrolysis and condensation. Hydrolysis is the process of adding water to a compound to break that compound down. In silica aerogels, the water is added to leave open OH groups which are attached to a metal, in this case silicon. The next step, condensation, is where water is removed, and M-O-M bridges are produced to link the particles together. These clusters then begin to link and combine in a colloidal suspension with each other to ultimately produce a larger body, eventually ending up as a gel. [2,3]

$$1)\ M^{+} + H_2O \rightarrow M\text{-}OH + H^{+}$$
$$2)\ M\text{-}OH \rightarrow O\text{-}M\text{-}O + (n)H_2O$$
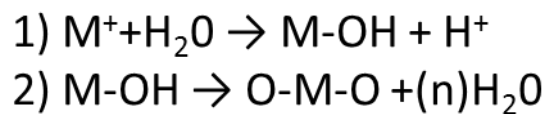
Figure 3. The equations for 1) hydrolysis (water is added) and 2) condensation (water is removed).

This second step is where the smaller clusters combine to produce the larger gel body, known as the gelation process. In this portion of the process the partials are lining up and combining in a three-dimensional grid. This can be seen in figure 4. This grid is the backbone of what will become an aerogel. In polymers, the particles simply begin to conglomerate producing the small particles, then these particles aggregate just as they would in a silica gel to produce the secondary particles. [21]

10
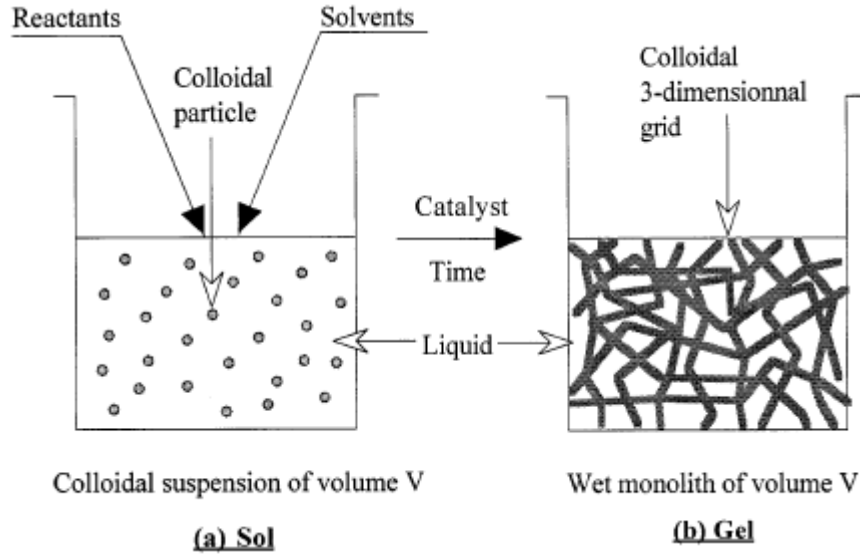
Figure 4. showing the transformation from sol to gel, taken from A. C. Pierre and G. M. Pajonk [3]

1.3) Drying Method History

The main issue with the fabrication of aerogel is the drying step. Due to the differential capillary forces this process becomes complex. The original method used to dry aerogel was evaporation. [1] Evaporation is when the solvent is removed by the simple process of atmospheric air drying. In this process cracking will typically occur. This can be seen in figure 5. As not all pores are the same size, the stress on one side of a pore wall and the other will be uneven, and this stress causes cracking. To remove capillary forces, the method of supercritical drying was developed. This method was first applied by Kistler in the 1930's. [1,3]

Figure 5. an image indicating the results of differential capillary forces. Supercritical liquids having zero surface energy, remove this stress; taken from A. C. Pierre and G. M. Pajonk [3]

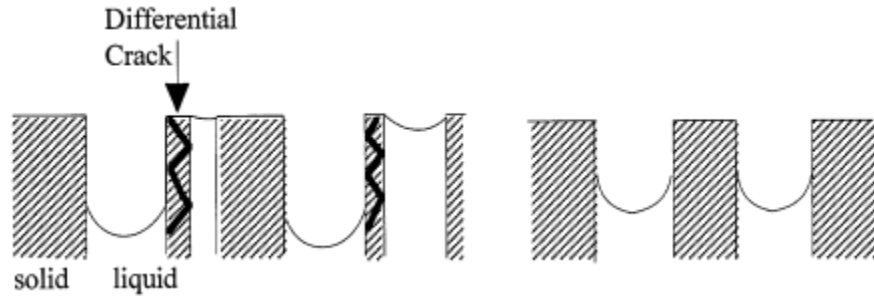The supercritical method is done by heating a gel in an enclosed autoclave until the temperature and pressure reach or slightly exceed the critical temperature T_c and pressure P_c of the liquid in the pores. [1-3] This is done because at supercritical temperature and pressures, the solvent within the pores can move freely as it will have a surface energy of zero. This eliminates capillary forces, and the fluid is free to flow out without damaging the monolith. [2] This will result in avoiding the pores from collapse. [22] After the critical temperature and pressure has been reached, the temperature and pressure are lowered back to ambient conditions. The temperature and pressure are lowered by removing the heat source (heating coils are turned off) and opening a venting valve to reduce pressure. The gel can then be removed from the vessel. [2] A common gas to be utilized in the autoclave for the solvent exchange, as well as what was used in this experiment, is CO_2. [3]

A less tested method of drying is freeze drying. Freeze drying uses sublimation, changing the solvent from a solid to a gas as shown figure 6. In theory it works, but the effectiveness of the drying has been debated. It is tough to produce a monolith that has avoided cracking during the freezing process. Many gels are broken down to a powder during drying. [23] This is due to the freezing prior to the drying process. Water inside of the monolith will expand causing the larger structure to crack and turn into a powder. [3]

12

Recently the effectiveness of the freeze drying method has been tested based on the length of time of freeze and the temperature of the chamber. [24] In an experiment done by T. Yamamoto et al. a mesoporous sol-gel material was frozen and dried at two different temperatures (243 K and 263 K) and frozen for a wide array of times ranging from 1 day to 20 days. The material was then weighed to determine if the solvent had been removed. It was determined that at 263 K the solvent would be removed in approximately 1 day. The lower temperature, 243K, would require between 5 and 10 days to fully remove the solvent from the pores. [24] This experiment shows that at higher temperatures the drying process will happen quicker. This observation can be explained by the exponential dependence of partial pressure on temperature.
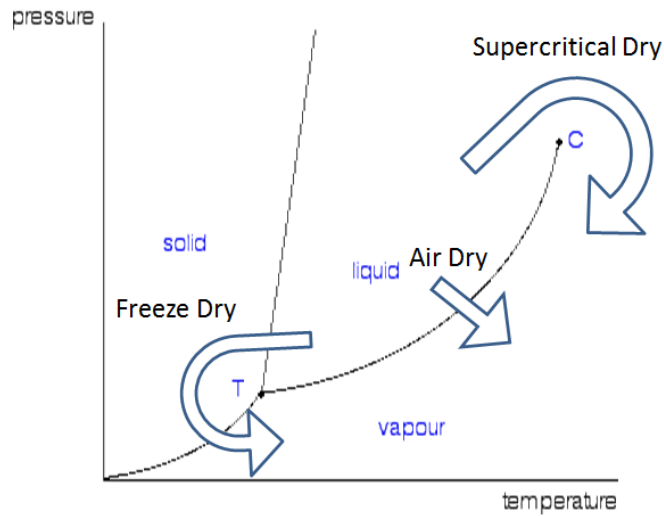

Figure 6. A phase diagram indicating the drying metods

1.4) Drawbacks

Each drying method has its own drawbacks. Although the air drying method is by far the simplest as it requires nearly no equipment or setup, it is done infrequently because it negatively affects the finished

materials. Due to the capillary forces on the skeletal structure during air evaporation, air drying can often result in highly cracked monoliths with high shrinkage. This results in the pores collapsing and producing xerogel, a much more compact gel than an aerogel with less desirable properties. [3]

The most common method of drying gels is supercritically drying. This method however, also comes with drawbacks. The supercritical drying process is long and tough to manage. The time required to dry gels supercritically can range from a minimum of 2-3 hours. [8] Due to the fact that supercritically dried gels require at least one solvent exchange, the time required for larger pieces of aerogel or foam to dry may take even longer still. [20] This slows down the production time. The bigger issue is that supercritical CO_2 must reach a temperature of 304 K and a pressure of 7.37 MPa. [3] The high pressure requires a pressure vessel with thick steel walls and no points of structural weakness. This is less of an issue for a small chamber where small pieces of material could be dried in a given time, but this limits the size of the materials that can be produced. To produce larger pieces of material a larger chamber would need to be constructed. A large steel chamber with no points of structural weakness would become incredibly expensive to produce. Determining a less costly method of drying gels has become important. [25]

The freeze drying method shares a similar issue with supercritical drying. It can also take a long time, up to 5-10 days at temperatures of 243K to fully freeze and sublimate the solvent out of nanoporous foam. [24] American Lyophilizer has calculated more rapid drying times even at low temperatures; however these times are noted to require secondary drying to remove residual moisture. [26] A benefit of freeze drying is cost (when compared to supercritical drying). The production of a vacuum chamber is much easier than the production of a chamber that can withstand a pressure and temperature required for supercritical CO_2.

14

1.5) 3D Printing

The 3D printing process has made it possible to produce a wide variety of materials in a wide variety of forms in the modern era. Invented in the 1980s by Charles Hull, the process was first designed by placing successive layers of material on top of each other to produce a 3D object. [27] 3D printing is considered an additive manufacturing and a solid freeform fabrication process. [28] Although producing parts on a large scale is still more economically efficient, in recent years 3D printing has become more popular due to its ability to make inexpensive custom parts. Commonly used with plastics, 3D printers are praised for their ability to cut costs on engineering of products. [29] For example, NASA was able to produce a custom fuel injector utilizing a 3D printer at a lower cost and in less time when compared to traditional methods. [27] 3D printing now expands beyond its original field to many other applications. [28] Common applications are art, and increasingly the medical field printing simple organs. [27] However, printing foams is uncommon. One example of foam printing is the complex method of high internal phase emulsion (HIPE). Porous polymers have been photopolymerized using this method. This method is a lithography-based additive manufacturing technology (AMT), where a growing sample is radiated with light from below and slowly dragged upward as it grows. The produced material is dubbed polyHIPE. [30] An objective of this project was to determine a simpler method to 3D print porous materials.

1.6) Objectives

The objectives of this project were to produce polymer nanofoam material by the process of photogelation. Aerogel material has been produced using this method, [8] so part of this experiment was to further investigate photogelation using only polymer. After gelation the next task was to determine the most effective method of drying for polymer foams as well as determining the effect of concentration and type of polymer on the properties of the foams. These drying methods were air

drying, supercritical drying, and freeze drying. Supercritical drying is often considered to be the drying method that leads to the materials with the best properties. [3] This experiment was also designed to see if air drying or freeze drying could also be effective drying techniques for nanoporous foams. The chosen materials HDDA and DPHA were used because of their differing reactivity; HDDA being difunctional, while DPHA is pentafunctional. The concentrations of polymer ranged from 6% - 50% by volume. Differing concentrations were used to determine which concentration on monomer would have the ideal properties for practical usage. The low concentrations of polymer were 15% for HDDA and 6% for DPHA. These concentrations were chosen as they were near the lowest amount of polymer required for polymerization. The higher ends (50% for HDDA and 20% for DPHA) were chosen because at higher concentrations of polymer the finished material would result in a core shell material. A core shell material is a material that does not have the same properties (density) on the inside and outside. After the materials were produced with a range of concentration of polymer and in all three drying methods, they were tested for their properties. The properties tested were density, Young's modulus, surface area, and particle shape of the secondary aggregates. This project was also designed to investigate ways to produce foam material in interesting geometries through the process of 3D printing.

Chapter 2: Experimental Section

2.1) Foam Synthesis

All gels were prepared using a method of 'one-pot chemistry' in 1.27 cm (0.5") diameter syringe tubes. The majority of gels were designed to be approximately 4.7 mL in volume. They were prepared using varying amounts of monomer to solvent ratios ranging from 6% - 50% monomer by volume. The monomers chosen were Hexanedioldiacrylate (HDDA) and Dipentaerythritol Hexaacrylate (DPHA) which are difunctional and pentafunctional monomers respectively. The structure of these monomers is shown in figure 7. All gels contained (including the polymer and solvent) eosin Y as a photo-imitator as well as methyldiethanolethylamine (Amine) as a co-photo-initiator. [8] The chosen solvent for both the air dried and supercritical dried gels was ethanol. For both the air dried gels and the supercritical dried gels the eosin Y was dissolved into the solvent prior to preparation. This eosin Y solution and amine were added to the mixture of monomer and solvent. After preparation the gels were placed in a Light Emitting Diode (LED) array of 6 LEDs, each with a wavelength peak of 532 nm and a power of 1 Watt. The LEDs were mounted on optical mounting posts and their height was set according to the center of the syringe tube containing the polymer solution. This was done to induce and generally took 30 minutes to 2 hours for the gels to fully polymerize. This LED set up is the same as L. S. White et al. [8] as seen in figure 8.
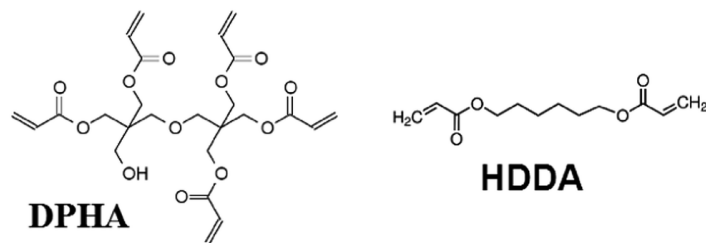

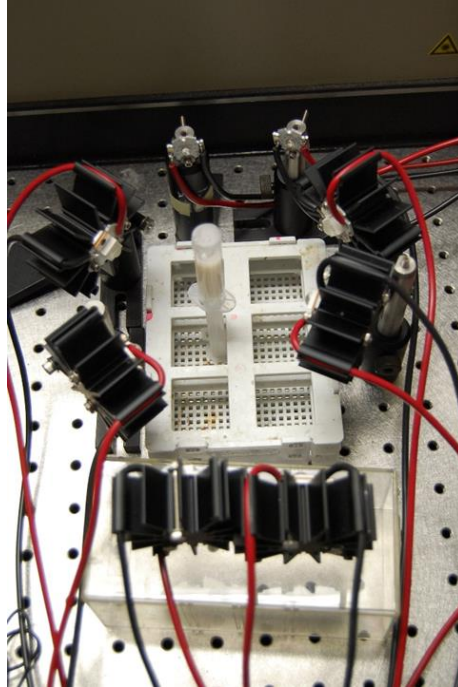**Figure 7.** Monomers used in the gels.

Figure 8. LED set up; taken from L. S. White et al. [8]

The freeze dried gels were prepared in the same general manner with a slight alteration. The first change was that the solvent choice was t-butanol due to its appropriate sublimation temperature and pressure. T-butanol has a triple point temperature of 299K at a pressure around 0.1 bar, cyclohexane has a triple point temperature of approximately 280K and a pressure around 0.1 bar, water has a triple point temperature of 273K at a pressure of 0.0061 bar. [31] Due to the comparatively high pressure of the triple point of t-butanol, it became the ideal choice to use for sublimation purposes. This is because it would not require as strong of a vacuum when compared to water.

Eosin Y was not added to the solvent prior to mixing of precursors for the samples that were to be freeze dried, due to the high freezing point of t-butanol. Small amounts of eosin Y (> 0.1 mg) dissolved directly into the precursors after mixing. This was done because it was much more practical to put powder eosin Y directly into the mixed precursors. The amine was added in the same manner. After

18

preparation the gels were placed under the LED display as they were for the other drying methods, and then removed after approximately 30 minutes to 2 hours when they had fully polymerized. The components of each gel can be seen in table 2.

Table 2. A table indicating the increment of precursors put into each foam.

Sample	ethanol (ml)	T-Butanol(ml)	HDDA (ml)	Amine(ml)	Eosin + (ml)	Eosin y (mg)
HDDA 20 AD	2.4	0	1	0.025	0.1	0
HDDA 30 AD	3.3	0	1.5	0.025	0.1	0
HDDA 37 AD	3	0	1.8	0.025	0.1	0
HDDA 50 AD	3.8	0	1	0.025	0.1	0
HDDA 15 SC	4.05	0	0.75	0.025	0.1	0
HDDA 30 SC	3.3	0	1.5	0.025	0.1	0
HDDA 37 SC	3	0	1.8	0.025	0.1	0
HDDA 50 SC	3.8	0	1	0.025	0.1	0
HDDA 15 FD	0	2.72	0.48	0.017	0	> 0.1
HDDA 20 FD	0	1.9	0.5	0.012	0.05	0
HDDA 30 FD	0	2.24	0.96	0.017	0	> 0.1
HDDA 37 FD	0	1.26	0.74	0.01	0	> 0.1
HDDA 50 FD	0	1	1	0.01	0	> 0.1

Sample	Ethanol (ml)	T-Butanol (ml)	DPHA Stock (ml)	Amine (ml)	Eosin + (ml)	Eosin y (mg)
DPHA 6 AD	2.625	0	2.07	0.025	0.01	0
DPHA 12 AD	1.415	0	3.29	0.025	0.01	0
DPHA 15 AD	0.988	0	3.71	0.025	0.01	0
DPHA 20 AD	0	0	4.7	0.025	0.01	0
DPHA 6 SC	2.635	0	2.07	0.025	0.01	0
DPHA 12 SC	1.415	0	3.29	0.025	0.01	0
DPHA 15 SC	0.988	0	3.71	0.025	0.01	0
DPHA 20 SC	0	0	4.7	0.025	0.01	0
DPHA 6 FD	0	1.41	1.79	0.017	0	> 0.1
DPHA 12 FD	0	0.96	2.24	0.017	0	> 0.1
DPHA 15 FD	0	0.67	2.5	0.017	0	> 0.1
DPHA 20 FD	0	0	3.2	0.017	0	> 0.1

*Eosin + is Eosin y disolved in ethonol 6 mg per 50 ml
*Solid Eosin was disolved into all freeze dried samples prior to polymerization (excluding HDDA FD 20)
*DPHA stock solution is 20% DPHA and 80% ethanol or T-butanol (by volume) depending on the drying method

19

2.1.1) Photopolymerization

Photopolymerization was chosen over other methods such as thermal polymerization as this method reduces evaporation of the solvent during polymerization. [8] In this method, green light (532 nm) from the LEDs is adsorbed by the photoinitiator (eosin Y). After the light is absorbed by the eosin Y dye, charge is transferred from the eosin Y to the coinitiator, the amine. This process results in the reduced radical in the dye, and the coinitiator radical becoming able to begin Photopolymerization. [8]

2.1.2) 3D Printer Setup

The 3D printed foams were produced by placing successive layers of material on top of each other. The precursors were mixed in a centrifuge tube and then extracted with a syringe that was to be used in the syringe pump. This syringe was then placed in a Harvard Apparatus model 11 syringe pump, which was set to extrude at 0.07 mL/min with an extruder opening of approximately 0.5 mm. The syringe was connected to a catheter to guide the precursors, ending in a cut pipette tip (with an opening of approximately 0.5 mm) to allow a constant drip of precursor. A larger opening would result in a larger drop of precursors. These larger drops would fall at a much less consistent rate and with larger areas resulting in a lower resolution of the finished material. The precursor was allowed to drip onto a glass slide mounted on an X-Y translation stage. While it was dripping the translation stage was set to move in a square shape that had a side length of 10 mm long at a rate of 0.25 mm/s. As the precursors drip downward toward the glass slide, the incident laser beam was being directed to the location the drops were landing. The laser was aimed to have an angle as close to 90° with respect to the glass slide as possible without interacting with the precursors until they had hit the slide as seen in figures 9 and 10. This process continued until the translation stage had made at least 20 full iterations. This repetition allowed for the growth of material that was approximately 1 mm in height. After the polymerization

process the finished 3D printed square was left to air dry for at least 12 hours. (See figures 9 and 10 for
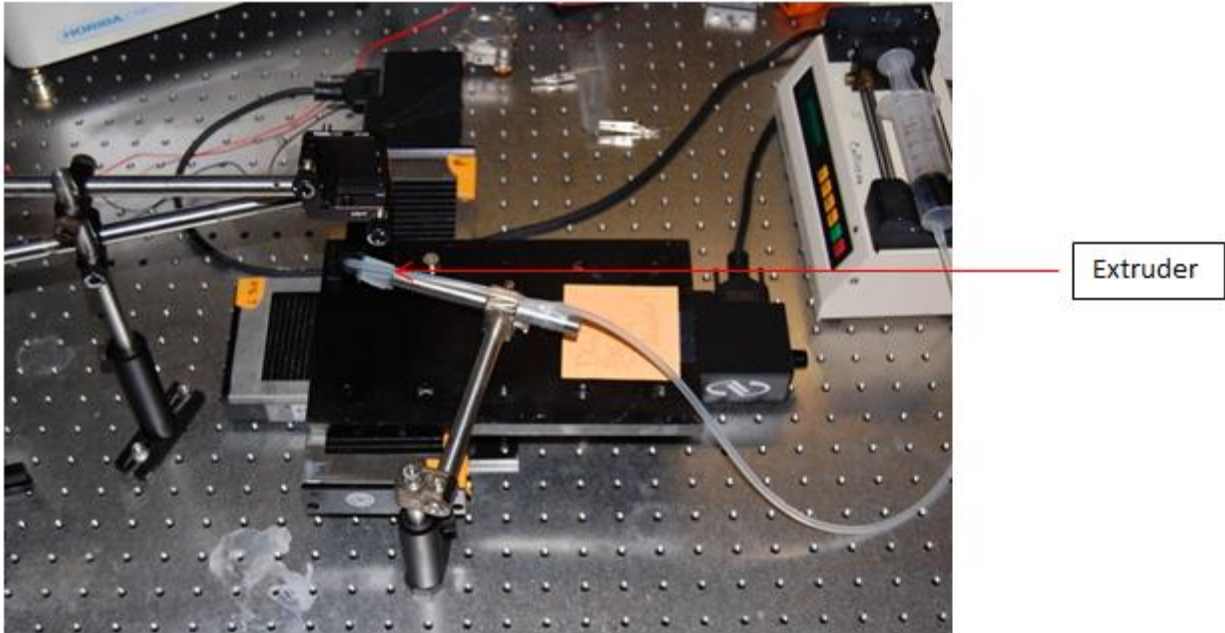
setup)

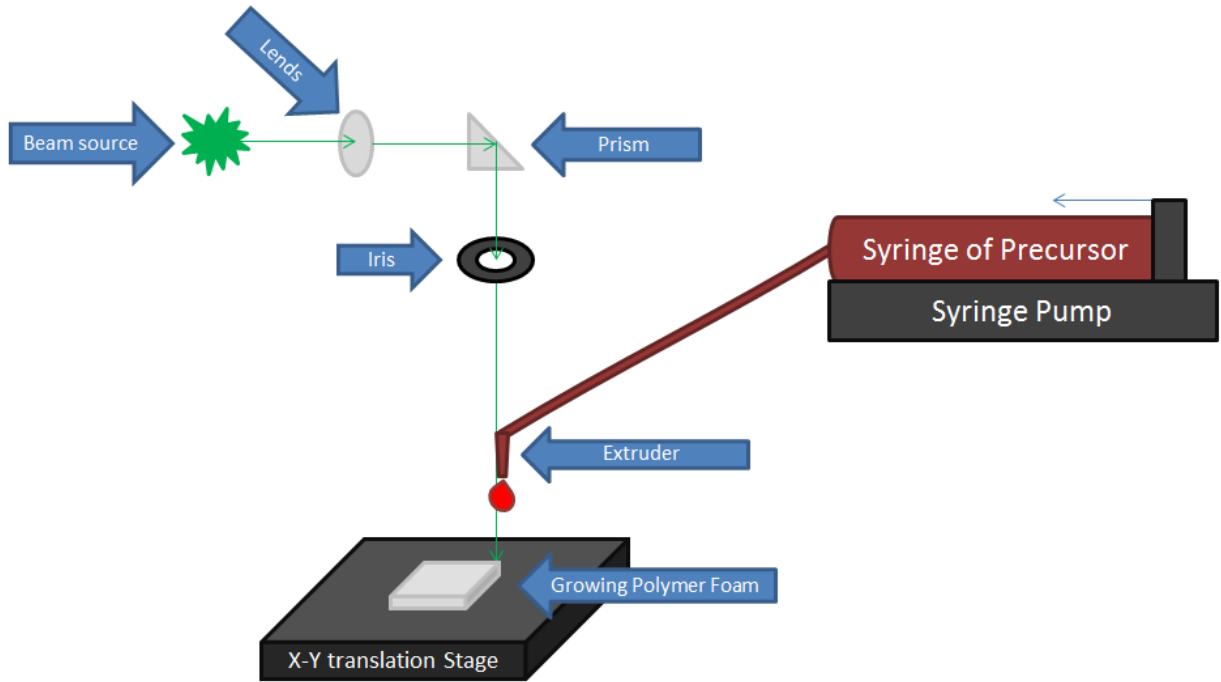**Figure 9.** Experimental setup for the 3D printing of the foams.

Figure 10. 3D printer setup

2.2) Drying Methods

The possible methods of drying are best illustrated by looking at a typical phase diagram of a solvent (figure 6). Air drying is the direct method of the solvent going from liquid to vapor. Supercritical drying is a method of drying that takes the solvent beyond its super critical point. Essentially the solvent goes from liquid, to supercritical, then to vapor. Freeze drying takes the liquid solvent, freezes it, and then removes the solvent via sublimation.

2.2.1) Air Drying

The air dried gels were left in a fume hood partially covered with parafilm while still in their syringe tubes. The partial cover was to avoid an overly rapid drying process, which would lead to further

cracking of the monolith. They were left for approximately 48 hours to ensure that all of the solvent had been removed. The 48 hour time was determined to be the ideal amount of time to wait through trial and error. If the wet gel was left for less than 48 hours there was often solvent left in the pores.

2.2.2) Supercritical Drying

In the process of supercritical drying, a sample is placed in a sealed chamber that will have its temperature and pressure raised just beyond the critical temperature T_C and critical pressure P_C of the solvent. This chamber is partially filled with ethanol and is monitored through a pressure gauge and a thermocouple (See 11). The sample will reach T_c and P_C after 1.5 hours. The temperature and pressure would then be held for 20 minutes. It is vented to remove the waste ethanol, and let cool for at least 4 hours to allow the sample to reach room temperature. The dried foam material can then be removed.
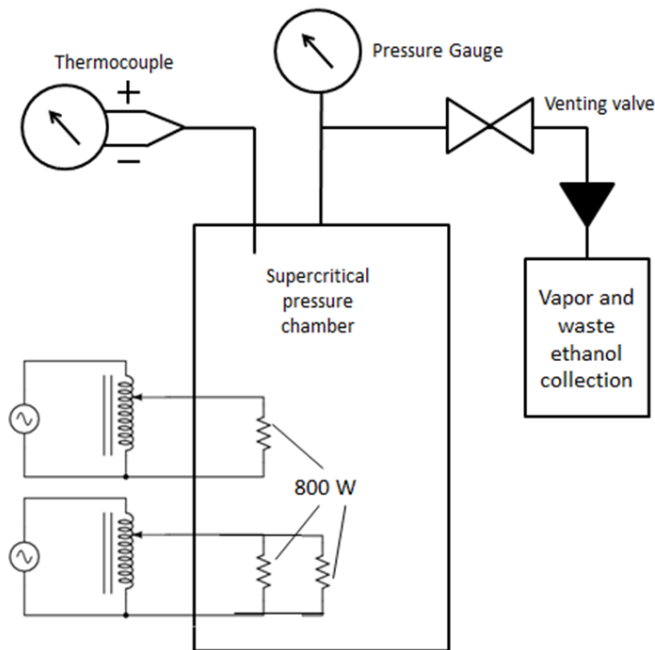

Figure 11. Diagram of supercritical drying chamber, with the smaller container being the waste ethanol.

2.2.3) Freeze Drying

Freeze drying is not a commonly used technique for drying aerogel material. Freeze dried aerogels, often called cryogels, make use of this less common technique. The basic concept of freeze drying is that the liquid is frozen first, and then is removed via sublimation. As the solvent is sublimated out, the capillary forces are avoided. [3,24] This allows the foams to maintain their shape without shrinkage, as they would in the supercritical drying method. Unfortunately, freeze dried gels and foams commonly crack and turn into powder in the freezing process. As the solvent crystalizes it puts stress on the skeletal structure. These stresses are caused as crystals nucleate within pores. The growing crystals will exert a force on skeletal wall. Often the crystal cannot exert back a large enough force, resulting in the breaking of the structure. A way around this is to cool the solvent so fast that it will not crystalize, but instead will vitrify, [32] which is when the solvent will cool so quickly that it will turn into an amorphous solid or a glass avoiding the crystallization process all together. Another issue is choosing the proper solvent; t-butanol is a popular option. [3,24]

The freeze dried samples were first placed in a freezer at a temperature of 250K for a minimum of 3 hours to ensure the solvent was frozen. After the 3 hours, the freeze drying process starts by placing a gel in a vacuum chamber submerged in an ice bath at a temperature of 273K. This chamber is then connected to a mechanical (belt drive) vacuum pump. (See figure 12) The chamber is evacuated to approximately 500 mTorr for 36-48 hours. After the drying time the, vacuum is broken, and the dried gels can then be removed.
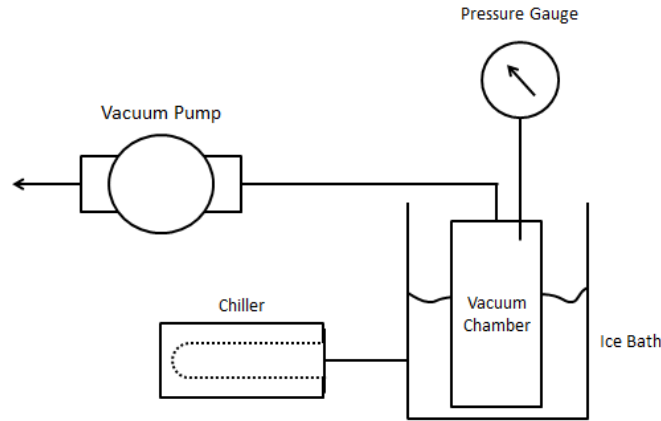
Figure 12. Diagram of freeze dryer

2.3) Characterization Methods

The properties of the dried material were tested by using the following characterization techniques. The techniques used were, density, modulus, surface area and porosity analyser, and SAXS (small angle x-ray scattering). The properties determined by each technique will be further explained in this section.

2.3.1) Density

The density of each gel was taken with the use of a caliper and an electronic scale. During the process of taking the density the shrinkage of the gels could be calculated, as all of the foams were produced in the same size cylindrical mold.

2.3.2) Modulus

Young's modulus, which is also known as elastic modulus, defines the relation between stress and strain.

$$E = \frac{\sigma}{\varepsilon}$$

Where E is Young's modulus measured in Pa, σ is stress measured in Pa, and ε is the strain. For this portion of the experiment the sample would be placed between two plates, the plate above the sample would begin moving downward, applying a normal force (See figure 13). As this force is increased the strain is measured and the stress-strain curve is produced. Using this curve Young's Modulus can be calculated by taking the slope of the first part of the curve, prior to the slope changing as the foam material compresses and becomes denser (see figure 14). The stress-strain curve was produced using a compression device, MTS Insight 30, with a load capacity of 30 kN. With a 30kN load capacity the pressure can reach approximately 2.36 MPa for a sample that that has a diameter of 1.27 cm (which is our maximum size of a sample given zero shrinkage).
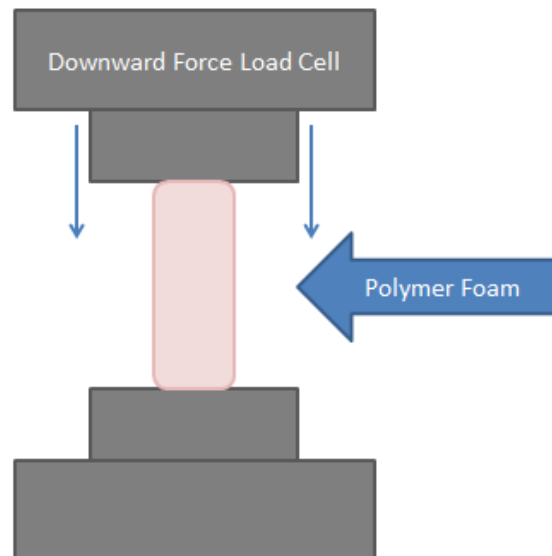

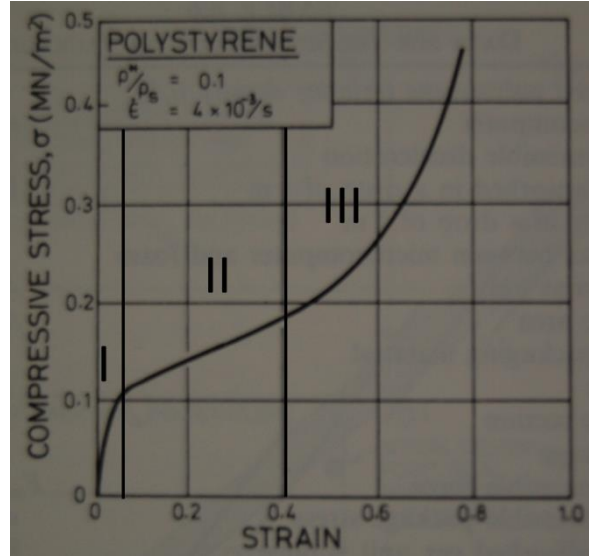**Figure 13.** Diagram of compression apparatus

Figure 14. A stress–strain curve of polystyrene foam, considered to be a near-optimum curve modified from L. J. Gibson [33]. The three regions indicate linear elasticity, cell collapsing, and densification respectively. [33]

2.3.3) BET

The Surface Area and Pore Size Analyzer device used in this experiment was a Quantachrome Autosorb. These devices are commonly referred to as BET, named after the creators of the theory, Brunauer–Emmett–Teller. The basic idea is that the more gas particles that can adsorb onto a material at a given pressure, the higher the surface area will be. See figure 15.
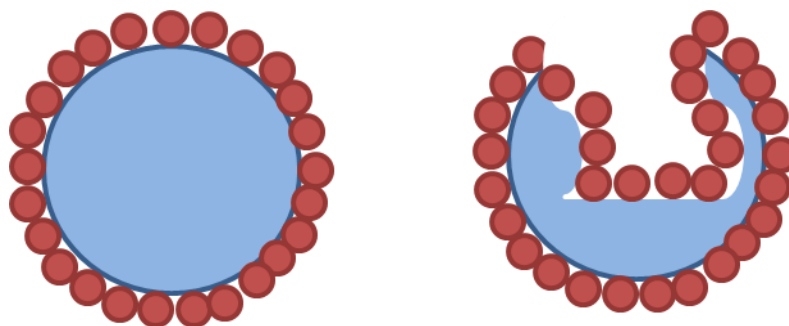
Figure 15. image indicating a large surface area results in more particles being able to adsorb to the surface. In this case a particle with a pore would have a larger surface area.

The theory behind BET is that gas inert molecules will adsorb to a solid, the adsorbed layers do not interact, and Langmuir theory applies to every layer. The Langmuir theory essentially states that an adsorbate acts as an ideal gas at isothermal conditions. [34] When a gas is adsorbed, it sticks to the surface of the material. The adsorbate, in this case N_2, is held to the surface by Van Der Waals forces. N_2 is chosen due to its unreactive nature and its low cost, however other adsorbates can be used such as Argon. To allow the N_2 to condensate on the surface the temperature needs to be low, so this process is done at a temperature of 77K.

The process of BET is done in a few steps. Initially the sample is prepared by taking a piece of the foam that is approximately 60 mg and cutting it into pieces that fit inside of the sample holder. These pieces are then put into the glass sample holder and attached to the degassing station. The sample must be degassed to remove any leftover solvent or water from the pores. The sample is placed in a glass tube and then, heated to 90° C under vacuum for a set period of time. For this experiment the time chosen was a minimum of 12 hours. After the degassing process, the sample is placed in a second station where the tube is submerged in liquid nitrogen. The tube is first evacuated, then it is filled at a determined pressure with the adsorbate. A flow meter measures how much adsorbate will go to the sample as gas

flows into the sample chamber. The process of vacuum and adsorbate filling is repeated several times with differing pressures of adsorbate.

 As more gas particles are adsorbed a monolayer is produced. This pressure is approximately 15% of the saturation pressure depending on the surface area of the material. [35] The volume of gas adsorbed is measured for pressures between 5% and 35% of the saturation pressure. The slope of the curve gives the surface area. An example of a produced curve can be seen in figure 16.
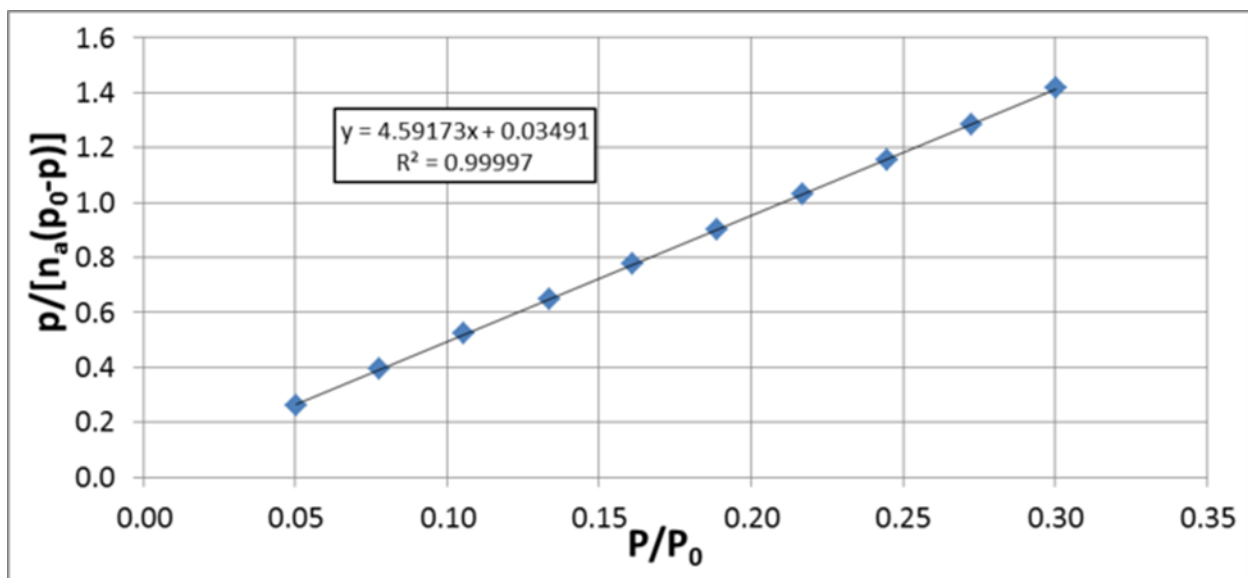

Figure 16. An example of an adsorption curve with 10 measurements taken. The x-axis is relative pressure, while the y-axis is volume of adsorbate. This curve gives enough information to determine the surface area. Taken from A. Connelly [36]

Surface areas were measured using five data points as this method has a higher accuracy, as opposed to measurements where only one data point is measured. Five data points are commonly considered to be sufficient for a surface area measurement. [35] Common surface area for supercritical dried polyurethane nanoporous foams fall in the range of 10-300 m^2/g. [5] This range was dependent on the type of polymer used in the synthesis as well as the concentration of polymer. For example supercritically dried

difunctional polyurethane foams with a concentration range of 9-22% polymer have a surface area in the range of 4-24 m^2/g. Supercritically dried trifunctional polyurethane foams with a concentration range of 9-22% polymer have a surface area in the range of 54-170 m^2/g. [5]

2.3.4) SAXS

Small Angle X-ray Scattering or SAXS was used to characterize the structure of the foam material. SAXS is a useful technique for amorphous materials. This is in opposition to XRD, which requires crystalline materials. [37] For both XRD and SAXS a copper filament with current running through has a large applied voltage (30-60 kV) between the filament and an anode. Electrons will hit the anode and produce X-rays. A large chiller keeps the anode from overheating. The X-rays, which are limited to one wavelength due to a monochromator, are directed through a system of collimators that limit beam divergence. The incident X-ray will interact with the sample and scatter in all directions elastically, that is without loss of energy. The X-rays scatter due to their interaction with the materials electron density. This process can be thought of like light interacting with a water droplet and the light scattering in many directions. The type of scattering depends on the type of sample. Particles such as dispersions and powders, which were used in this experiment, will have an isotropic scattering pattern. A single crystal will have a perfectly oriented scattering pattern. Other particles, such as fibers and some sheared liquids, will have a partially oriented scattering pattern. [38] After the X-rays have interacted with the material the refracted X-rays will reach the detectors, which measure the intensity of the beam. There is a beam stop behind the sample that the un-scattered beam will hit. The beam stop is to prevent the highest intensity portion of the beam from directly hitting the detector. Direct contact could either damage the detector or cause back scatter that would negatively affect the data. [38] The basic set up of SAXS can be seen in figure 17.
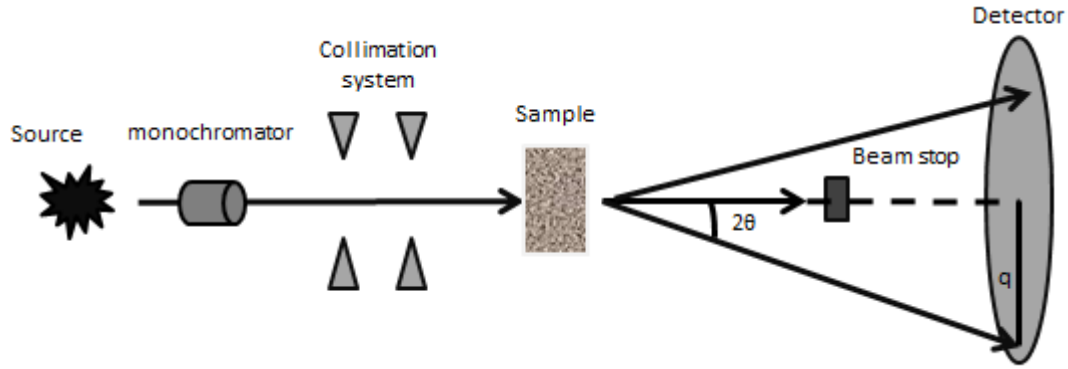
Figure 17. SAXS set up

The distribution of scattering is angle dependent. The distribution is intensity as a function of q which is to make scattering patterns independent of the wavelength and angle. q, as seen in figure 17, is a function of the wavelength λ and the angle θ. It is measured in nm^{-1}. Often q is described as the scattering vector or momentum transfer. [38]

$$q = \frac{4\pi}{\lambda} \cdot \sin\theta$$

By measuring this distribution the particle size and structure can be determined. The size of the particle is determined by where the slopes change on the graph, while the shape of the particle is determined by the slope. The initial slope is the aggregate particles, while the later slope is the smaller primary particle. The slope of the log-log curve determines the shape, a slope of P<3 is mass fractal, 3<P<4 is a surface fractal and P>4 is a smith sphere. [37] Some slope dependent shapes can be seen in figure 18.
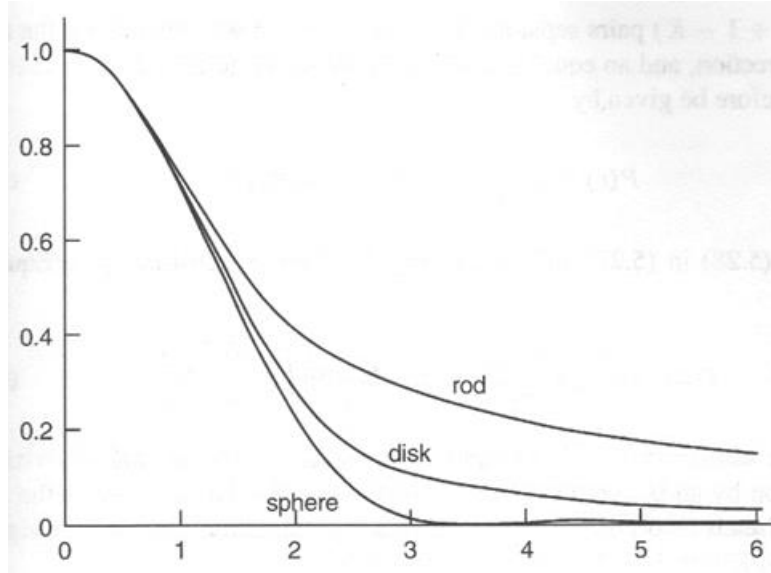
Figure 18. indicating different slopes will have different shapes, rods P=1, disks P=2, and spheres p=4. Taken from M. Bertino [39]

After the distribution is produced the particle structure can be calculated. The Beaucage Model is frequently used for aerogel and foam material. [5]

$$I_{Beaucage}(Q) = G \exp\left(-\frac{Q^2 R_g^2}{3}\right) + B \exp\left(-\frac{Q^2 R_{sub}^2}{3} \left(\frac{[\text{erf}(QkR_g/\sqrt{6})]^3}{Q}\right)\right)^P + G_s \exp\left(-\frac{Q^2 R_s^2}{3}\right)$$
$$+ B_s \left(\frac{[\text{erf}(Qk_s R_s/\sqrt{6})]^3}{Q}\right)^{P_s}$$

The first term gives the first portion of the fit, giving a point of maximum intensity. The second term gives the first portion of the slope, the shape of the agglomerate particles. Finally the last term gives the slope (shape) of the smaller particles. [40] As seen in figure 19, when a parameter is changed in the Beaucage Model, even in large amounts, there is often there is no change in the fit line. Note P, the second to last parameter in figure 19. This commonly occurs with these multi-parameter fits.
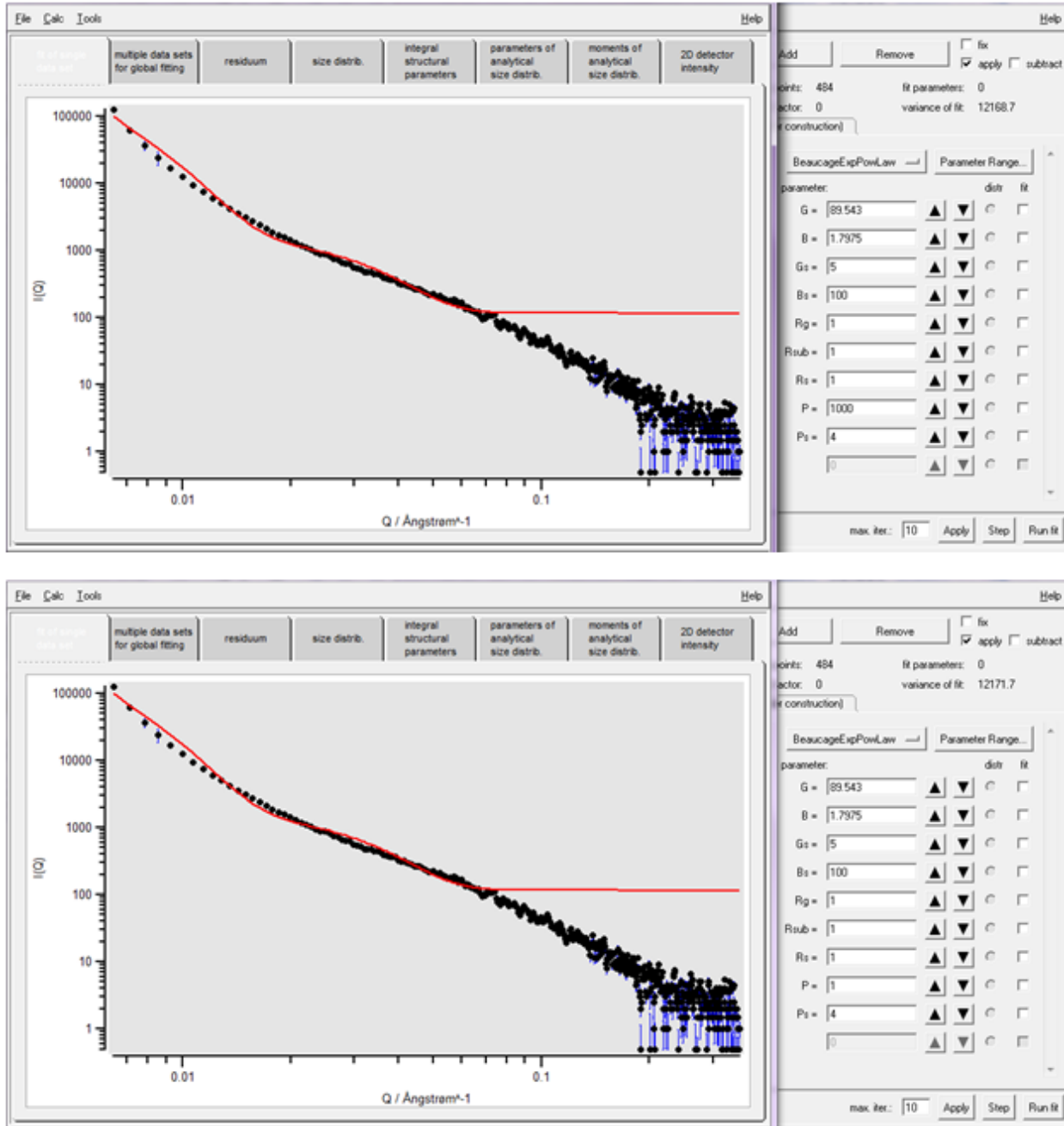
Figure 19. Indicating the difficulties of multi fit parameters (Note the second to last parameter P). Even with a large change in the parameter P, there is no change in the fit of the slope. P, the final exponent in the second term had changed by a factor of 3 with no change in the slope.

The traits that can be calculated using the Beaucage Model are the size and shape for both for the individual particles and the conglomeration of the particles. [38] A program such as Sasfit utilizes a number of parameters the main noted parameters; are Rg, Rs, P, and Ps. Rg is the large scale structure of the particles. Rs is the size of the sub units. P describes the power law associated with the larger structure. Finally Ps describes the power law associated with the smaller structure. The power P and Ps determine the shape of the particle (Figure 18). The other factors, G, B, Gs, Bs are simply pre-factors. All of these factors are the parameters of the Beaucage Model.

Chapter 3: Results

3.1) Density

The density as expected for both HDDA and DPHA would increase with the amount of polymer. This can be seen in figure 20. The drying method did not appear to have a large effect on density. Typically, the supercritical drying method lead to the lowest density of the foam material, and the air drying method lead to the highest density. However, this change was small and may not be attributed to the drying method. This can be seen in figure 21. The polymer concentration and the drying method had little to no correlation to the percentage of shrinkage. This can be seen in figures 22 and 23. The density ranges fell between 0.13- 0.89 g/cm^3 for HDDA. The highest density went to the highest concentration of polymer (50%). At this concentration the center of the material had a different density than the outer layer and became core shell. The range of density for DPHA foams fell between 0.16- 0.36 g/cm^3, as the polymer ratio for DPHA never topped 20% and the densities were kept lower. Densities can be seen for both HDDA and DPHA in table 3. In either case, when compared to polyurethane foams, the densities are within reason. Densities from polyurethane foams with a polymer concentration in the range of 9-22% were reported in the range of 0.12- 55 g/cm^3. [5] Shrinkage for both materials, excluding a few outliers, was approximately 10% throughout the experiment; this can be seen in table 4. There did not appear to be any major correlation between the drying method, polymer type or concentration of polymer on the shrinkage. Linear shrinkage for supercritically dried polyurethane foams has been reported with a range of approximately 10-25%. [5] Acrylics, such as HDDA and DPHA have not been investigated greatly enough to compare data.

Table 3. chart comparing the effect of percent of polymer and the drying method for both HDDA and DPHA on the density; % polymer is by volume.

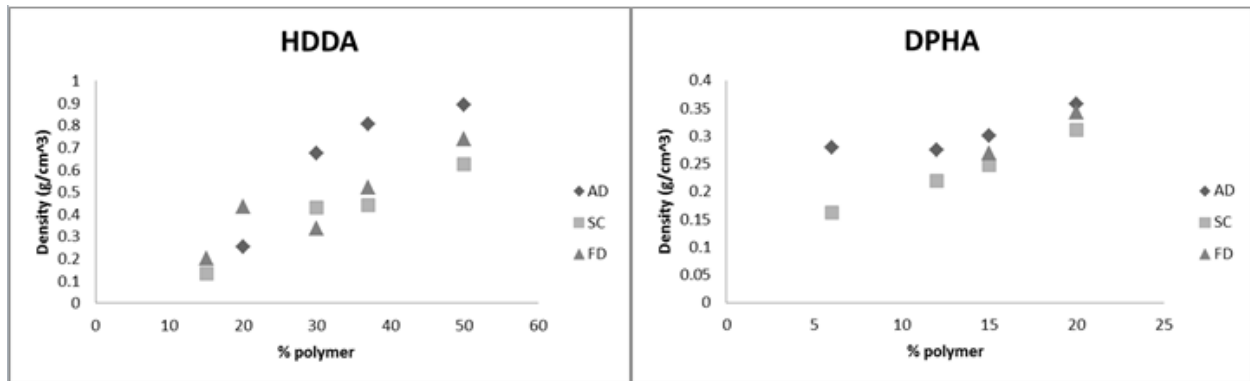| Density (g/cm^3) of HDDA foams				Density (g/cm^3) of HDDA foams			
% polymer	drying method			% polymer	drying method		
	AD	SC	FD		AD	SC	FD
15	N/A	0.131915	0.201057	6	0.280041	0.162501	N/A
20	0.254	N/A	0.43159	12	0.275575	0.220028	N/A
30	0.672403	0.42886	0.333966	15	0.301071	0.24809	0.270089
37	0.804325	0.440878	0.518888	20	0.357532	0.31137	0.343242
50	0.89	0.62463	0.736976				

Figure 20. comparison for density for each drying method for both HDDA and DPHA. It can be seen that drying method causes little variation on density and for both materials the density increases with the concentration of polymer.
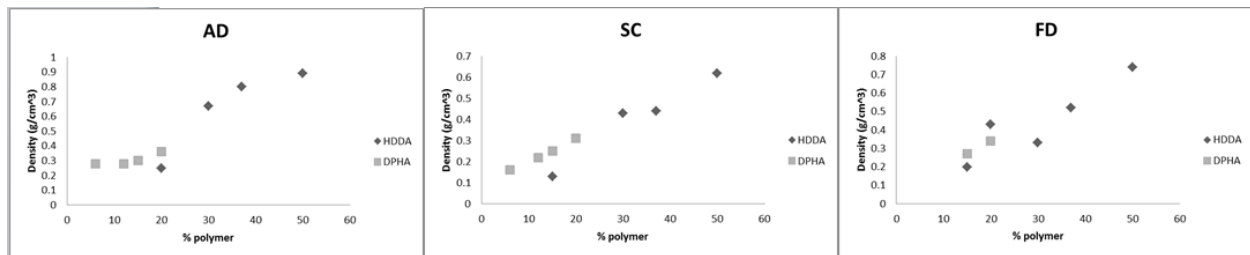

Figure 21. comparison of density for polymers used in all three drying methods. It can be seen that the type of polymer used has little effect on density. Density depends on polymer concentration for the most part.

Table 4. chart comparing the effect of percent of polymer and the drying method for both HDDA and DPHA on the shrinkage; % polymer is by volume.

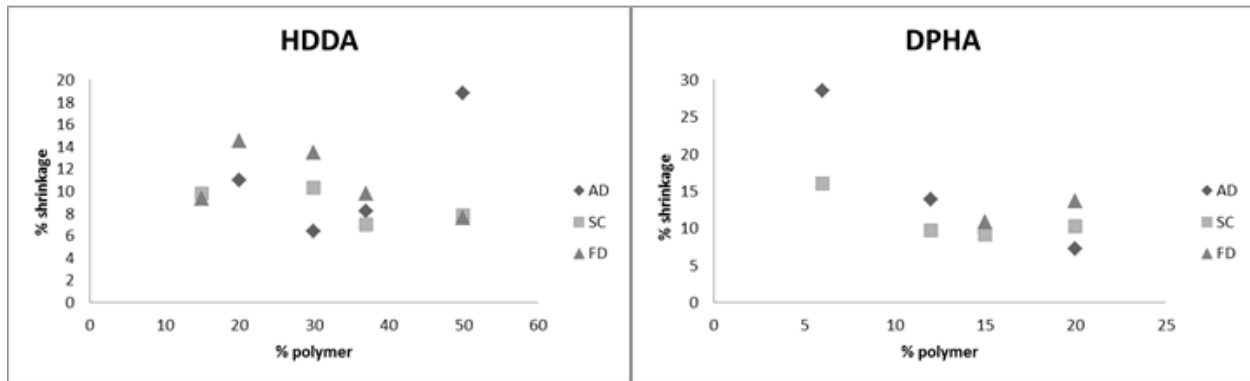| Shrinkage % for HDDA foams				Shrinkage % for DPHA foams			
% polymer	drying method			% polymer	drying method		
	AD	SC	FD		AD	SC	FD
15	N/A	9.8	9.3	6	28.5	16	N/A
20	11	N/A	14.5	12	13.9	9.7	N/A
30	6.4	10.3	13.5	15	9.4	9.2	10.8
37	8.2	7	9.8	20	7.2	10.3	13.7
50	18.8	7.8	7.6				

Figure 22. comparison of the shrinkage for each drying method for both HDDA and DPHA. It can be seen that drying method and type of polymer causes little variation on shrinkage
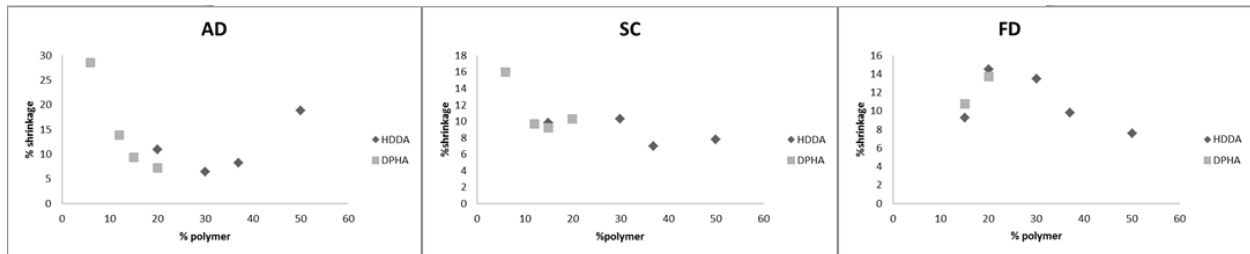

Figure 23. comparison of the shrinkage of the foam material by polymer type. It can be seen that the type of polymer used has little effect on the shrinkage.

3.2) Modulus

During the compression process a stress-strain curve was produced. This stress-strain curve can be broken into multiple regions as seen in figure 14. The first region is linear elasticity, which is where the modulus is taken. The next is plateau, which is the portion of compression where the cell walls are

collapsing. Next is densification, which is where cell walls are touching. [33] Finally the structure breaks in the final region as seen in figure 26.
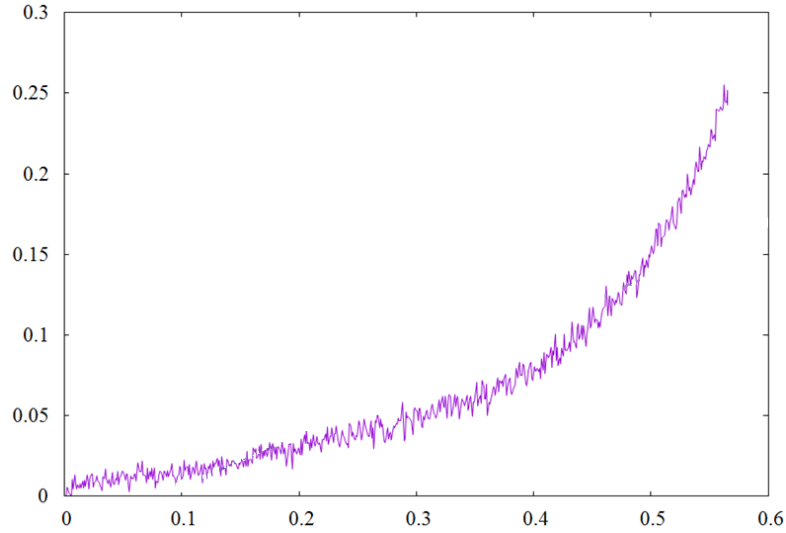

Figure 24. The stress-strain curve for HDDA 15 FD. The x-axis is strain which is dimensionless and the y-axis is stress in Pascals. This material never reached its breaking point and had a shallow stress- strain curve.
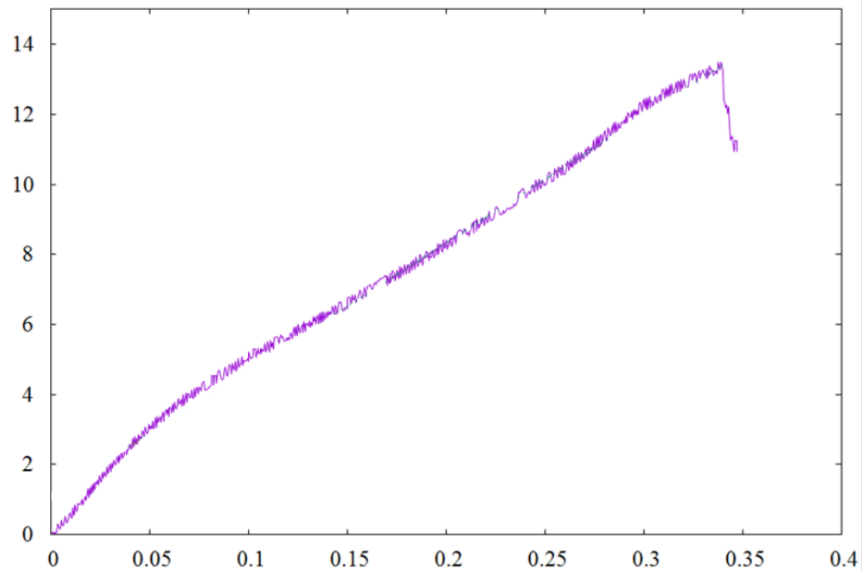

Figure 25. The stress strain curve for HDDA 37 FD. The x-axis is strain, which is dimensionless, and the y-axis is stress in Pascals. Note the breaking point around 13 Pascals.
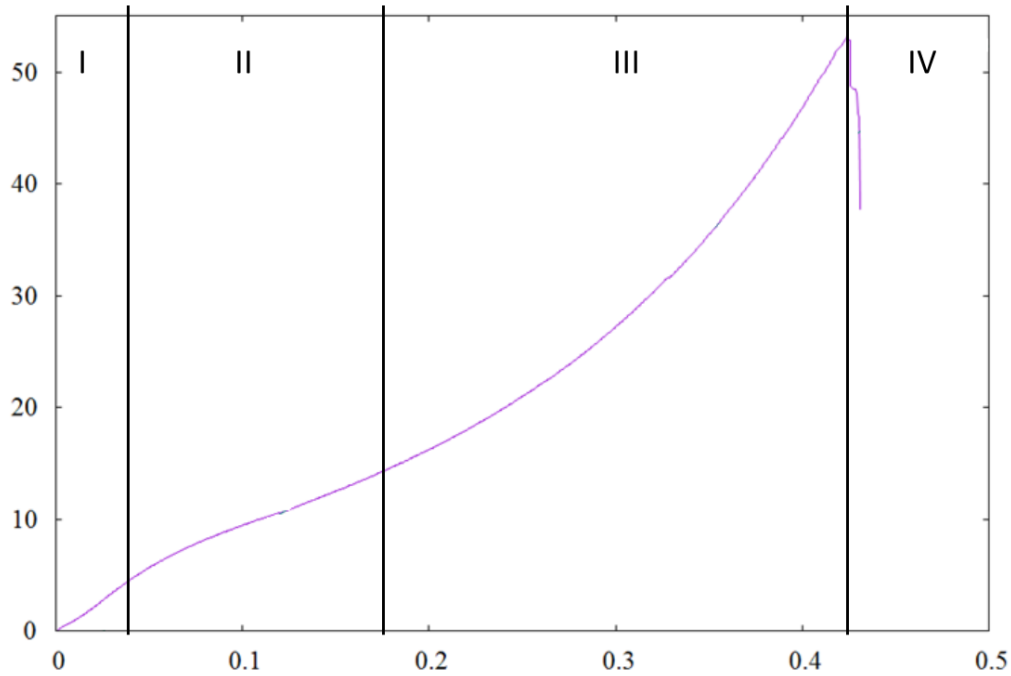
Figure 26. The stress strain curve for HDDA 50 FD. The x-axis is strain which is dimensionless, and the y-axis is stress in Pascals. Note the higher breaking point around 50 Pascals. Region I is linear elasticity, where the modulus is calculated. Region II is the plateau region, where the cells are collapsing. Region III is the Densification region where the cell walls begin to contact each other. Region IV is where the monolith had a break in structure. [33]

Using this data the modulus could be found by calculating the initial slope (region 1). The slope was calculated using a script for the program gnuplot. [41] The calculated moduli, as expected, were higher with higher polymer content. This also shows that there is a correlation between the densities of the material and the modulus, which was an expected correlation. The higher the density of the material, the higher the modulus will be. The drying method did not appear to have an effect on the modulus, with one exception. The freeze dried DPHA gels had a higher modulus than their air dried and supercritical dried counterparts.

The power law relation between modulus and density is largely dependent on the connectivity of the particles. Lower connectivity will have a higher exponent, as a low connectivity will have a low modulus at a low density. However, as the density is increased these low connectivity materials will become

thicker resulting in a rapid modulus growth. High connectivity materials already had a higher modulus to begin with, resulting in a less rapid increase in modulus with an increasing density. [15] The increase of modulus as a function of density can be seen in figures 28 and 29. For both HDDA and DPHA the modulus increases exponentially with a density that has a factor between 3 and 5.25. This is agreeable with supercritically dried silica aerogel material with polymer support. In a study done by L. S. White et al. [15] the modulus increased exponentially with density that has a factor 4.5. The connectivity explains why the HDDA had a higher exponent than DPHA, as HDDA is difunctional and would have made fewer connections than the pentafunctional DPHA. This can be seen in figure 27, the 'ball and stick' model describing connectivity. [42] An object of low connectivity with only one or two connections will be more easily deformed than a material with a higher increment of connections.
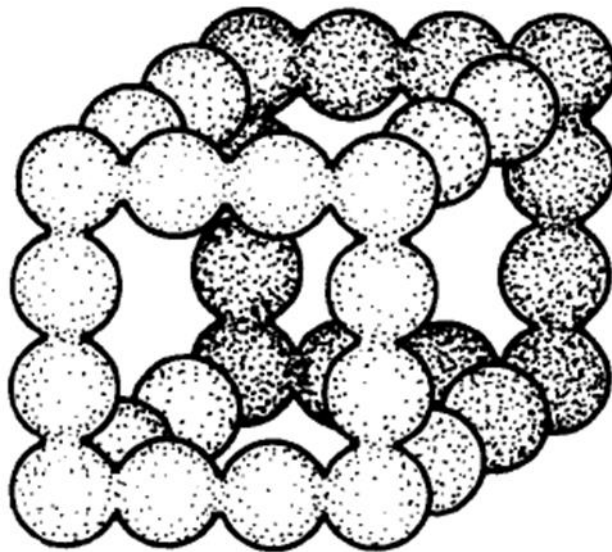

Figure 27. A 'ball and stick' model describing the connectivity of particles. Taken from T. Woignier [42]

Table 5. chart comparing the effect of percent of polymer and the drying method for both HDDA and DPHA on the Modulus; % polymer is by volume.

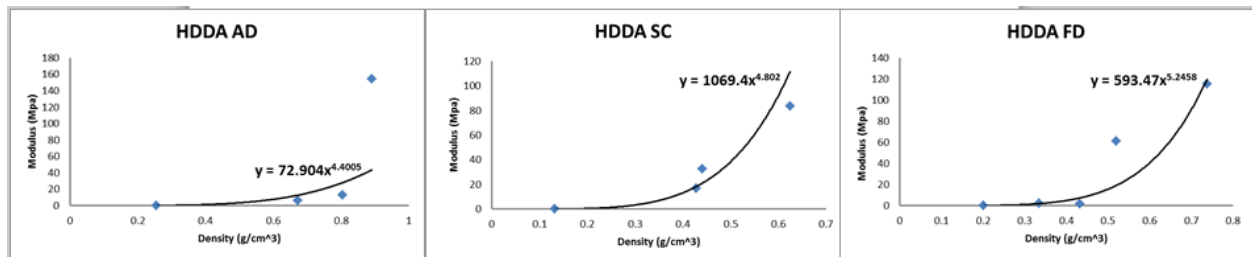| Modulus (Mpa) of HDDA foams				Modulus (Mpa) of HDDA foams			
% polymer	drying method			% polymer	drying method		
	AD	SC	FD		AD	SC	FD
15	N/A	0.058841	0.166203	6	0.282241	0.020591	N/A
20	0.218678	N/A	1.72223	12	0.169761	0.107673	N/A
30	6.24679	17.0146	2.01247	15	0.26754	0.127639	1.07997
37	12.9057	32.6028	61.1187	20	0.461054	0.263827	1.17961
50	154.288	83.8471	115.541				

Figure 28. The modulus as a function of density for HDDA foams. All have an exponent between in the range of 4.4 – 5.25. This is higher than DPHA.
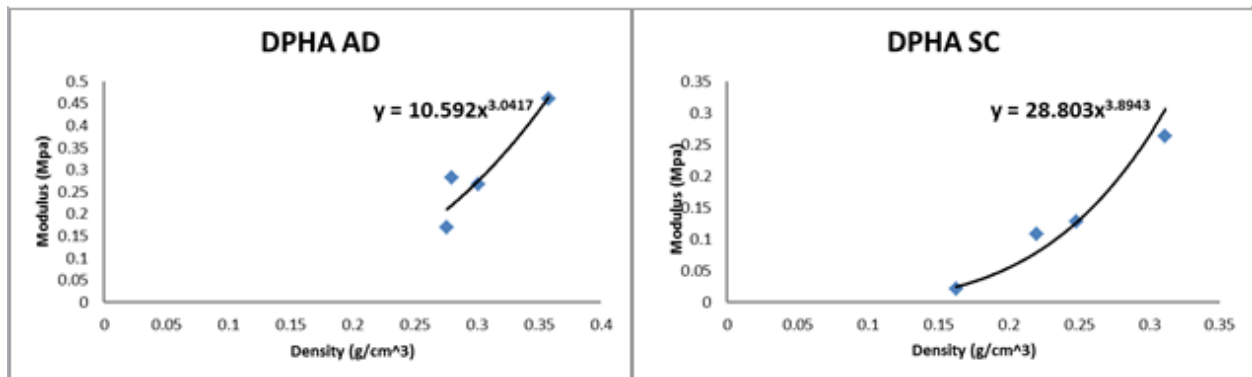

Figure 29. The modulus as a function of density for DPHA foams. They have exponents in the range of 3 – 4. Note that there is no curve for the freeze dried samples, there was not enough data to produce an appropriate curve.
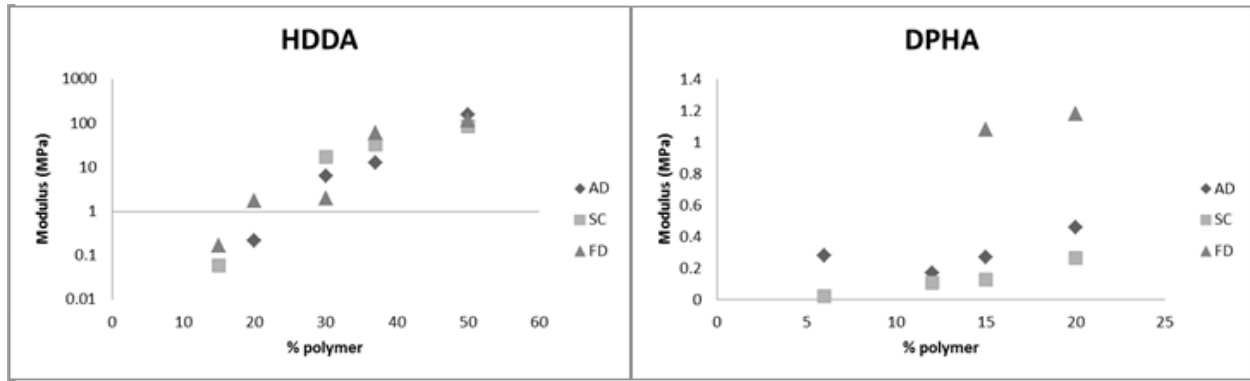
Figure 30. comparison of the modulus for each drying method on for HDDA and DPHA. It can be seen that drying method causes little variation on modulus for HDDA. However the FD method did result in a modulus higher by a factor of 10. In both cases the modulus increases with increasing concentration of polymer.
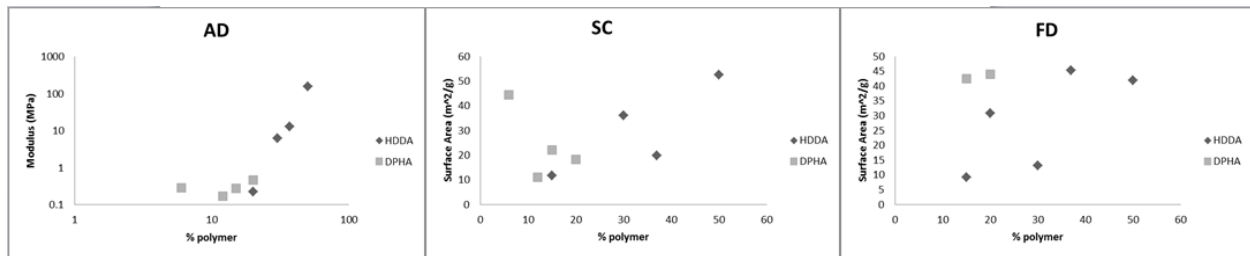

Figure 31. comparison of modulus, by the type of polymer used in all three drying methods. It can be seen that the type of polymer used has little effect on modulus. The higher concentration of polymer resulted in a higher modulus. Note the air dried plot is logarithmic.

3.3) BET

Surface area depended mostly on the concentration of polymer. The change in concentration of the polymer had a different effect for different polymers. In general, HDDA would have an increasing surface area with increasing polymer content. This was not so for DPHA. The DPHA gels would, in general, have a decreasing surface area with increasing polymer content. The drying method did not appear to have an effect on the surface area. The ranges of surface areas were between 10-60 m^2/g. The lower range surface area polyurethane samples, by Leventis et al. [5], would fall approximately in this region.

The higher surface areas would likely have more pore space, thus being better thermal insulators. This would indicate that a higher concentration of HDDA in foam precursors would be ideal for insulation application. This is excluding the upper limit of polymer concentration. Many of the 50% HDDA samples became core shell and their porosity dropped as a result. Contrarily DPHA would become a better insulator at lower concentrations.

Table 6. chart comparing the effect of percent of polymer and the drying method for both HDDA and DPHA on the surface area; % polymer is by volume.

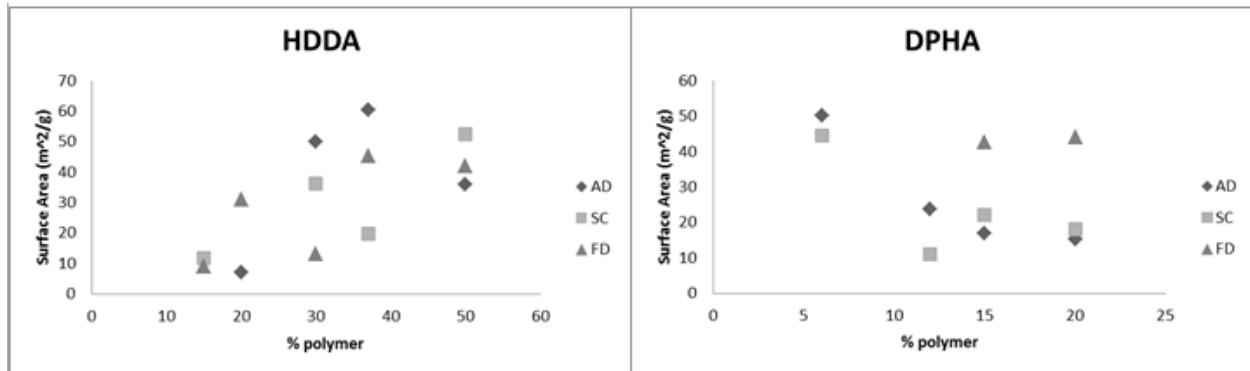| Surface Area (m^2/g) of HDDA foams				Surface Area (m^2/g) of DPHA foams			
% polymer	drying method			% polymer	drying method		
	AD	SC	FD		AD	SC	FD
15	N/A	11.74	9.146	6	50.22	44.4	N/A
20	7.221	N/A	30.9	12	23.84	11.13	N/A
30	49.9	36.2	13.15	15	16.98	22.09	42.59
37	60.36	19.8	45.24	20	15.27	18.23	44.05
50	36.1	52.49	42.03				

Figure 32. comparison of surface area method for both HDDA and DPHA. It can be seen that drying method causes little variation on surface area for both materials.
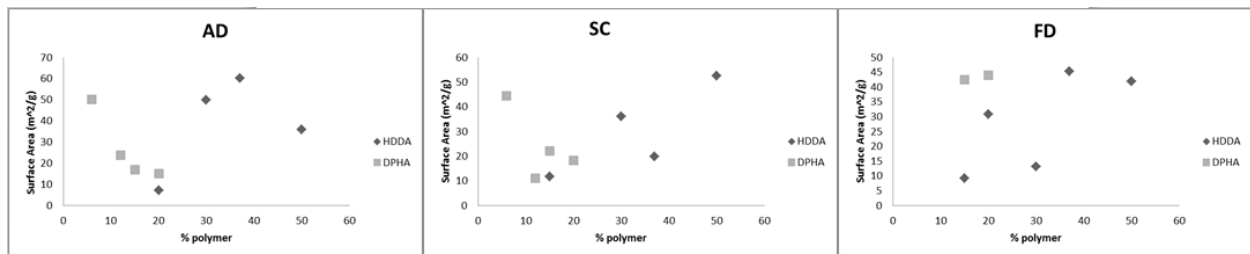

Figure 33. comparison of surface areas of the foam material by the polymer type. It can be seen that the type of polymer had an effect on the surface area. While the values are not too different, HDDA had an

43

increasing surface area with an increasing polymer concentration. On the other hand DPHA had a decreasing surface area with an increasing polymer concentration.

3.4) SAXS

Figure 34 shows the fits of two samples with the same polymer and the same drying method, DPHA and Supercritical drying respectively. The change between the two is the concentration of polymer. This indicates that the amount of polymer in a sample does not change the shape of the structure.

Figure 35 shows three samples of the same polymer and concentration of polymer. In this case both are DPHA. The difference between the samples was the drying methods AD (air dried), SC (supercritically dried) and FD (freeze dried). Again the data indicates no large change between the samples. This indicates that the drying method has no effect on the shape of the particles.

The ultimate take away was the slope of the curves or the parameter 'P' from the Beaucage model. This exponent tells us the shapes of the larger aggregate structure; in general this slope was in the range of 3.5>P>4.1. This slope is generally associated with a smooth spherical structure, [37] which is expected as many types of foam production result in a spherical shaped particle. [9] This indicates that these polymer foams structure are similar to those of other polymer foams. Leventis reported an initial slope of P≈4 as well for polyurea foam material [5].

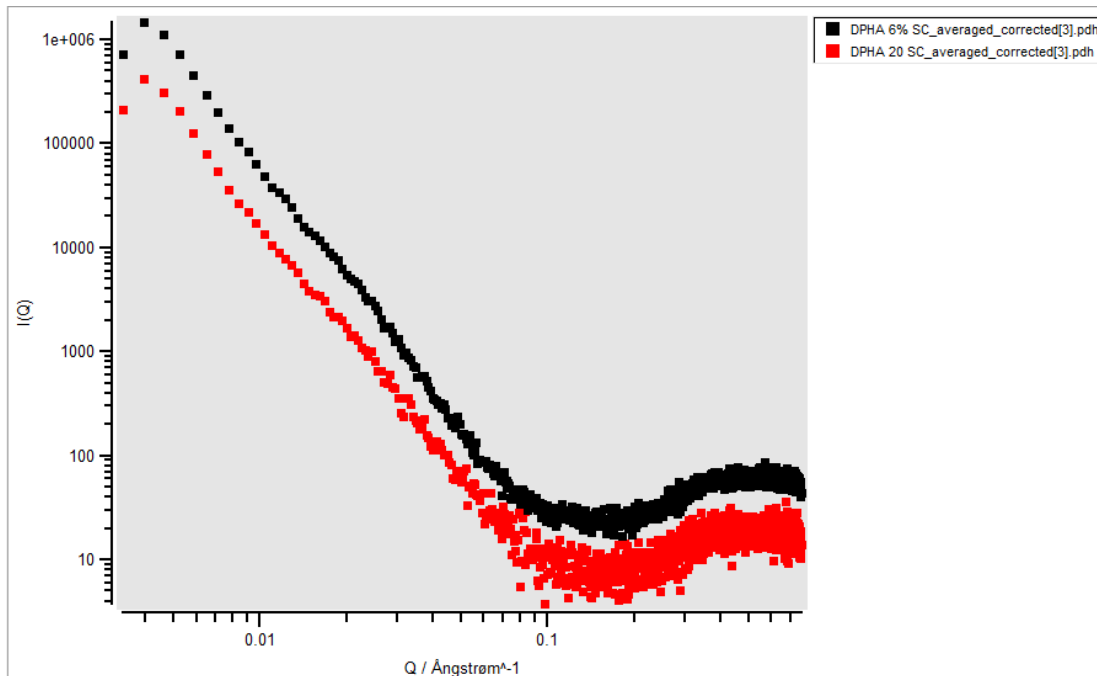**Figure 34.** Comparing two concentrations of polymer on SAXS, The slopes are approximately the same with a change in slope at the same point on the x-axis.
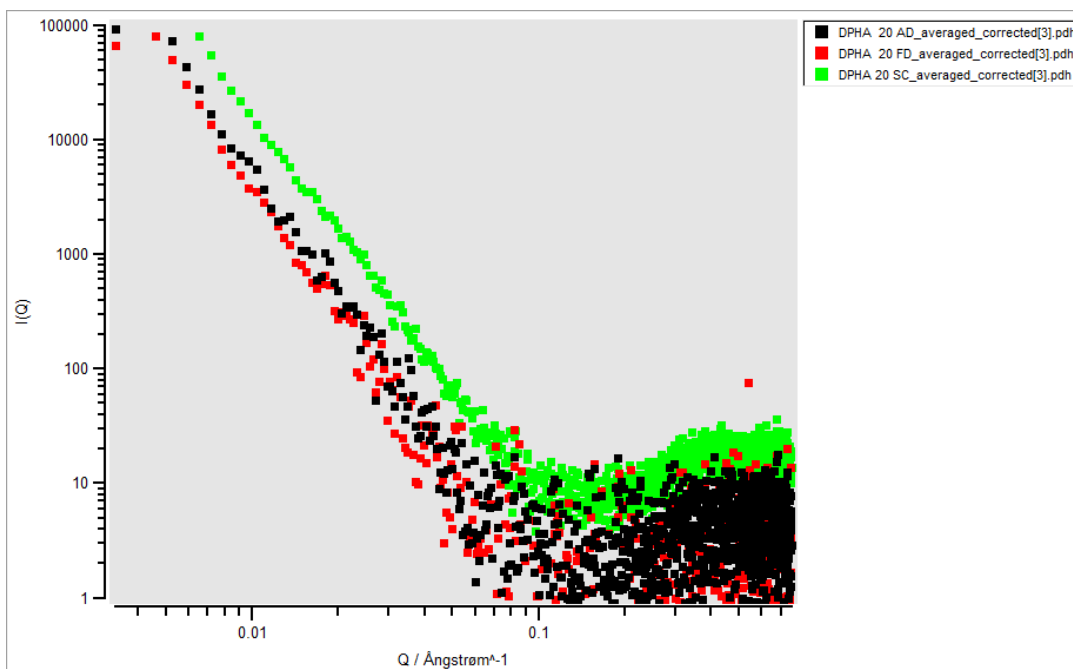

Figure 35. Comparing the three drying methods on SAXS. The three drying methods had approximately the same slope with a change in slope at the same points on the x-axis. This indicates the drying method does not affect the shape of the particles or the aggregates.

3.5) Drying Methods

3.5.1) Air Drying

As expected, the air dry method resulted in some problems with shrinkage, in particular the gels with a low polymer concentration. Although shrinkage was a problem, the other characteristics of the gels did not seem to change. They all maintained similar modulus and surface areas when compared to the gels of the same polymer concentration that were dried utilizing other methods. The largest fault with this method was that a larger percentage of samples would have cracks in the monolith after the drying process. DPHA samples that were low concentration polymer were the most commonly cracked materials.

3.5.2) Supercritical Drying

The supercritical drying method had the fewest instances of cracking, and also gels could be produced that would have minimal shrinkage even at low polymer content. This was the expected result as reported by the study that done by N. Leventis et al. [5]

3.5.3) Freeze Drying

The freeze drying method had a few flaws. The most notable was that some gels would contain residual solvent. This problem could be easily rectified by placing the gels in an oven for a short time after the drying process; this process did not appear to have an effect of the strength or the structure of the gels. The second major issue was similar to the issue with the air drying method. The DPHA gels would crack and turn to dust at a low concentration of polymer (below 15%). They also appeared to be more brittle than their supercritically dried counterparts. This did not appear to be a problem with the HDDA gels, which shows that HDDA is an excellent candidate as a freeze dryable polymer. This could be because HDDA is only difunctional. A difunctional molecule will be less cross-linked than a pentafunctional

molecule (DPHA). The less cross-linked material should be more flexible and able to withstand the freeze

drying process.

Chapter 4: Conclusions

4.1) Freezing Method

Both HDDA and DPHA monomers could be air dried, supercritically dried and freeze dried to remove the solvent. The methods did not seem to differ in the materials density, modulus, surface area or the shape of the particles in the material. As expected, with a higher concentration of monomer came a higher density and modulus, having exponential trends with exponents of 5.2 for HDDA. The surface area was found to increase with the concentration of monomer in HDDA, while the surface area of the monomer was found to decrease with an increasing concentration of monomer in DPHA. Based on the SAXS data, the shapes of the particles larger structures were consistently spheres or surface fractals. This is agreeable to the aerogel material made by Tamon [37], which had aggregate particles that were surface fractals. Polyurea foam material made by Leventis [5], however had both fractals and initial slopes of 2 indicating cylinders. The only major differences in this drying method were freeze drying low concentration DPHA foams. These foams would crack or turn to powder shortly after being removed from the chamber.

4.2) 3D Printing

It has also been shown that there is a capability to 3D print these nanoporous polymer foams using our method. The top down slow extruding method with a translation table is a plausible method to print these foams. It was shown that the faster polymerizing DPHA was much more promising for the 3D printing method. HDDA would take too long to polymerize and turn to an amorphous partially polymerized material. The DPHA gels, due to their more rapid polymerization, could be used to make clearer cut lines and shapes (see figures 36 and 37). This process, while effective, was time consuming. The production of a 5mm x 5mm square (after 35 circuits) took approximately 1 hour.
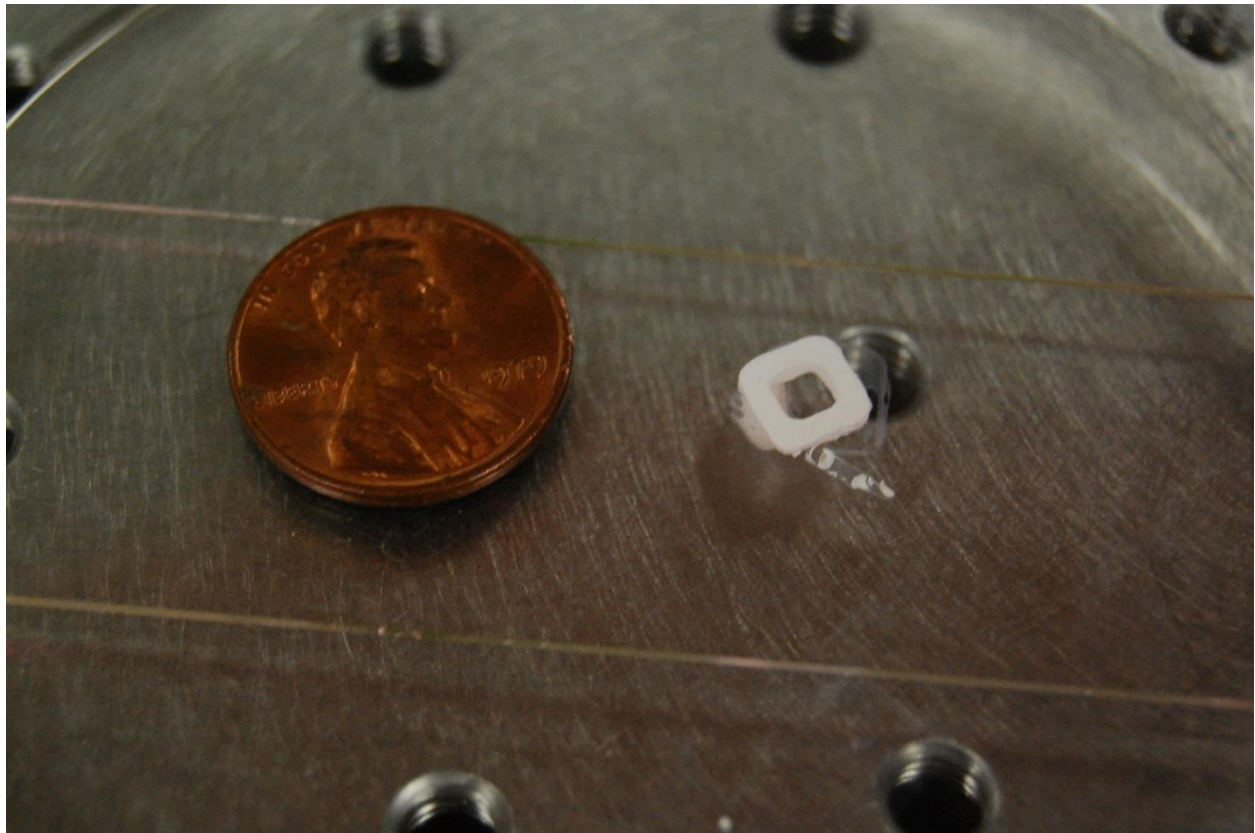
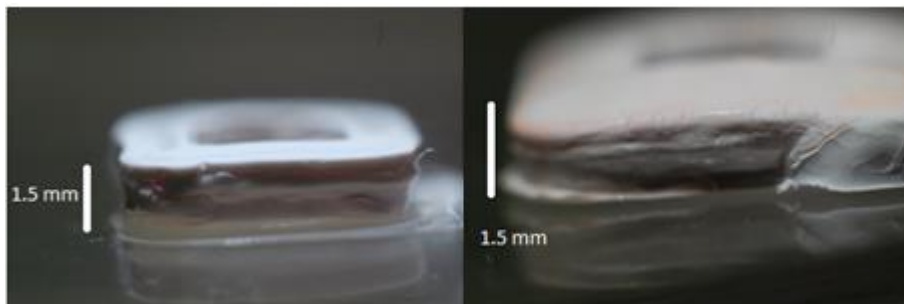**Figure 36.** Image of 3D printed DPHA material with a penny for scale.

Figure 37. Close up images of 3D printed air dried DPHA material.

4.3) Freeze Drying Poly-Urea

Desmodur 3200 and 3300 (structure in figure 38) were also shown to be a gel that could be freeze dried well. These samples were made to compare our drying method to already existing research on the more common supercritical drying method while using the same material. This was important as there is little in the literature about acrylics, which was the main focus of this study.
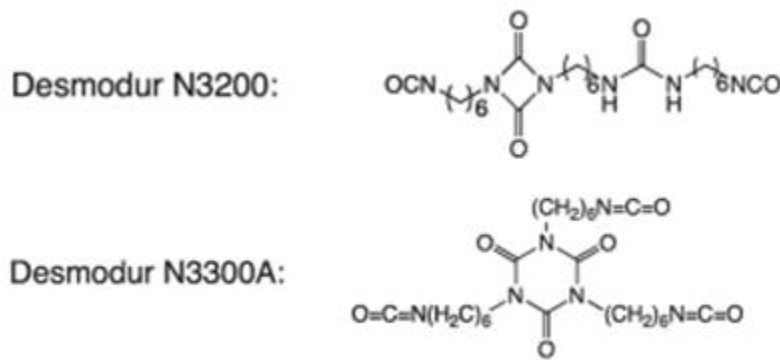

Figure 38. Polyurea monomers used in the gels. Taken from Leventis et al. [5]

These Desmodur gels could be polymerized in acetone without the need for a photo-catalyst. Simply adding amine at room temperature is sufficient to initiate polymerization; the polymerization was thermally initiated. The gels then required going through solvent exchange from the acetone to cyclohexane or t-butanol. The gels could then be freeze dried under the same conditions as the acrylic gels (HDDA and DPHA). Initial tests indicate t-butanol is a better solvent for the drying process, as the sample that used cyclohexane as a solvent did not fully dry. This is possibly due to the slightly higher triple point temperature of cyclohexane when compared to t-butanol. The Desmodur 3200 samples that were produced were tested for density and surface area. One larger sample, Poly U 15%, was also tested for modulus. The concentration of precursors can be seen in table 7**.** The results can be seen in table 8.

Table 7. A table indicating the increment of precursors in each foam.

Sample	Acetone (ml)	Desmodur 3200 (ml)	Amine(μl)	Water (μl)
Poly U 12.5%	0.875	0.125	2	2
Poly U 15%	2.55	0.45	8	8
Poly U 20%	0.8	0.2	2	2

Table 8. This table shows the results from the freeze dried polyurea samples. The measured surface areas of these samples were slightly lower than the supercritically dried gels produced and measured by Leventis et al. [5].

Sample name	density (g/cm^3)	Surface area (m^2/g)	Modulus (Mpa)
Poly U 12.5%	0.351	0.75	N/A
Poly U 15%	0.211	3.812	4.443
Poly U 20%	0.424	12.002	N/A

Table 9. Values for Desmodur 3200 reported by Leventis et al. [5]

Percent Polymer	density (g/cm^3)	Surface area (m^2/g)	Modulus (Mpa)
8.90%	0.175	4	N/A
13%	0.37	12.8	N/A
22.70%	0.54	23.6	N/A

Ultimately, the freezing method was tried with three different monomers. The first monomer used, DPHA, could only be frozen and removed from the chamber if there was a large concentration of monomer. This is due to the more ridged matrix of the penta-functional monomer. The next material used was HDDA. This material resulted in a monolith that did not crack or turn to a powder. The final materials that were used were Desmodur 3200 and 3300. Both of these materials were used in an experiment by Leventis et al. [5] the difference was that they were supercritically dried samples. They both could be frozen and produced a nice monolith. This, however, came at the cost of requiring solvent exchange, so these materials needed to use acetone as a solvent then to be exchanged to t-butanol. The solvent exchange process takes up more time and materials. This leads to the conclusion that HDDA is the most appealing polymer for freeze drying as it resulted in an un-cracked monolith as well as requiring no solvent exchange.

5.   References

1)   A. C. Pierre in: M.A. Aegerter, N. Leventis, M.M. Koeberl, M. Prassas (Eds.), Aerogels Handbook, Springer, New York, 2011, pp. 3-18.

2)   J. Fricke, Sci. Am., 1988, 92-97

3)   A. C. Pierre and G. M. Pajonk, Chem. Rev., 2002, **102**, 4243-4265

4)   L. White, Research seminar, 2016

5)   N. Leventis, C. Sotiriou-Leventis, N. Chandrasekaran, S. Mulik, Z. J. Larimore, H. Lu, G. Churu and J. T. Mang, Chem. Mater., 2010, **22**, 6692-6710 DOI:10.1021/cm102891d

6)   C. Forest, P. Chaumont, P. Cassagnau, B. Swoboda, P. Sonntag, Prog. Polym. Sci., 2014, **41(2015)**, 122-145

7)   W. R. Palani Raj, M. Sasthav, H. M. Chung, J. Appl. Polym. Sci., 1993, **49**, 1453-1470, DOI: 10.1002/app.1993.070490813

8)   L. S. White, M. F. Bertino G. Kitchen, J. Young, C. Newton, R. Al-Soubaihi, S. Saeed, K. Saoud, J. Mater. Chem. A, 2015, **3**, 762-722

9)   S. Orsi, E. Di Maio, S. Iannace, P. A. Netti, Nano Research, 2014, **7(7)**, 1018–1026, DOI:10.1007/s12274-014-0465-4

10)   L. Chen, D. Rende, L. S. Schadler, R. Ozisik; J. Mater. Chem. A, 2013, **1**, 3837-3850, DOI:10.1039/C2TA00086E

11)   C. Forest , P. Chaumont , P. Cassagnaua, B. Swoboda , P. Sonntag , Prog. Polym. Sci., 2015, **41**, 122-145, DOI:10.1016/j.progpolymsci.2014.07.001

12)   L. Verdolotti, M. Lavorgna, R. Lamanna , E. Di Maio, S. Iannace, Polymer, 2015, **56**, 20-28

13)   A. M. Scamardella, U. Vietri, L. Sorrentino, M. Lavorgna and E. Amendola, J. Cell. Plast., 2012, **48(6)**, 557-576, DOI: 10.1177/0021955X12445405 http://cel.sagepub.com/content/48/6/557.full.pdf+html

14)   A. Bureiko, A. Trybala, N. Kovalchuk, V. Starov, Adv. Colloid Interfac., 2015, **222**, 670-677, DOI:10.1016/j.cis.2014.10.001http://www.sciencedirect.com/science/article/pii/S00018686 14002644

15)   L. S. White, M. F. Bertino, S. Saeed and K. Saoud, Micropor. Mesipor. Mat., 2015, **217**, 244-252, DOI:10.1016/j.micromeso.2015.06.019

16)   A. M. Scamardella, U. Vietri, L. Sorrentino, M. Lavorgna, E. Amendola, J. Cell. Plast., 2012, **48(6)**, 5578-576

17)   L. Weigold, G. Reichenauer, J. of Non-Cryst. Solids, 2014, **406**, 73-78 DOI:10.1016/j.jnoncrysol.2014.09.040

18)   M. Wiener, G. Reichenauer, S. Braxmeier, F. Hemberger, H.-P. Ebert, Int. J. Thermophys, 2009, **30**, 1372–1385, DOI 10.1007/s10765-009-0595-1

19)   C. Chidambareswarapattar, Z. Larimore, C. Sotiriou-Leventis, J. T. Mang, N. Leventis, J. Mater. Chem., 2010, **20**, 9666-9678

20)   L. S. White, D. R. Echard, M. F. Bertino, X. Gao, S. Donthula, N. Leventis, N. Shukla, J. Kośny, S. Saeed and K Saoud, Transl. Mater. Res., 2016, **3**, 015002

21)   E. Kiran, J. of Supercrit Fluids, 2016, **110**, 126-153

22) J. Estella, J. C. Echeverria, M. Laguna, J. J. Garrido, J. Porous Mater., 2008, **15**, 705-713, DOI:10.1007/s10934-007-9156-9

23) G. W. Scherer, J. of Non-Cryst. Solids, 1993, **155**, 1-12, DOI:10.1016/0022-3093(93)90467-C

24) T. Yamamoto, T. Nishimura, T. Suzuki, H. Tamon, Carbon, 2000, **38**, 2374-2375

25) H. Tamon, H. Ishizaka, T. Yamamoto, T. Suzuki, Carbon, 2000, **7**, 1099-1105

26) American Lyophilizer, General Principals of Freeze Drying (The Lyophilization Process), 2016

27) C. Schubert, M. C. van Langeveld, L. A. Donos, Brit. J. Ophthalmol., 2014, **98**, 159-161, DOI:10.1136/bjophthalmol-2013-304446

28) M. Stanic, B. Lozo, D. G. Svetec, Rapid Prototyping J., 2012, **18(2)**, 120-128

29) T. Wohlers, Comput. Aided Eng., 1996, 8, 68

30) M. Sušec, S. C. Ligon, J. Stampfl, R. Liska, P. Krajnc, Macromol. Rapid Comm., 2013, **11**, 938-942, DOI: 10.1002/marc.201300016

31) NIST Database

32) G. W. Scherer, J. of Non-Cryst. Solids, 1992, **155**, 1-25

33) L. L. Gibson and M.F. Ashby, Cellular Solids, New York, 1988, pp. 120-167, 238.

34) I. Langmuir, J. Am. Chem. Soc., 1918, **40**, 1361.

35) Quantachrome. The Gas Sorption Process. Boynton Beach, FL: Quantachrome, 2007. Autosorb-1 Series. Quantachrome Instruments, 2007. Web. 2016.

36) A. Connelly, A Brief Guide to BET, 2015

37) H. Tamon and H. Ishizaka, J. Colloid Interf. Sci., 1998, **206**, 577-582

38) H. Schnablegger and Y. Singh, The SAXS Guide. 3rd ed. Austria: Anton Paar GmbH., 2013.

39) M. Bertino, Scattering, 2016, 30

40) J. Kohlbrecher, User guide for the SASfit software package, 2014

41) Sorceforge, Gnuplot Version 5.0, 2015, https://sourceforge.net/projects/gnuplot/files/

42) T. Woignier, J. Phalippou, J. Non-Cryst. Solid,s 1988, **100**, 404.